

Multi-parameter lead optimization to give an oral  
checkpoint kinase 1 (CHK1) inhibitor clinical  
candidate: (*R*)-5-((4-((morpholin-2-  
ylmethyl)amino)-5-(trifluoromethyl)pyridin-2-  
yl)amino)pyrazine-2-carbonitrile (CCT245737).

*James D. Osborne,<sup>†</sup> Thomas P. Matthews,<sup>†</sup> Tatiana McHardy,<sup>†</sup> Nicolas Proisy,<sup>†</sup> Kwai-Ming J. Cheung,<sup>†</sup> Michael Lainchbury,<sup>†</sup> Nathan Brown,<sup>†</sup> Michael I. Walton,<sup>†</sup> Paul D. Eve,<sup>†</sup> Katherine J. Boxall,<sup>†</sup> Angela Hayes,<sup>†</sup> Alan T. Henley,<sup>†</sup> Melanie R. Valenti,<sup>†</sup> Alexis K. De Haven Brandon,<sup>†</sup> Gary Box,<sup>†</sup> Yann Jamin,<sup>§</sup> Simon P. Robinson,<sup>§</sup> Isaac M. Westwood,<sup>†</sup> Rob L. M. van Montfort,<sup>†</sup> Philip M. Leonard,<sup>‡</sup> Marieke B. A. C. Lamers,<sup>‡</sup> John C. Reader,<sup>‡</sup> G. Wynne Aherne,<sup>†</sup> Florence I. Raynaud,<sup>†</sup> Suzanne A. Eccles,<sup>†</sup> Michelle D. Garrett,<sup>†</sup> Ian Collins,<sup>†,\*</sup>*

<sup>†</sup> Cancer Research UK Cancer Therapeutics Unit and <sup>§</sup> Division of Radiotherapy and Imaging,  
The Institute of Cancer Research, London, SM2 5NG, U.K.

<sup>‡</sup> Sareum Ltd, Cambridge, CB22 3FX, U.K.

## ABSTRACT

Multi-parameter optimization of a series of 5-((4-aminopyridin-2-yl)amino)pyrazine-2-carbonitriles resulted in the identification of a potent and selective, oral CHK1 preclinical development candidate with *in vivo* efficacy as a potentiator of deoxyribonucleic acid (DNA) damaging chemotherapy and as a single agent. Cellular mechanism of action assays were used to give an integrated assessment of compound selectivity during optimization resulting in a highly CHK1 selective, adenosine triphosphate (ATP) competitive inhibitor. A single substituent vector directed away from the CHK1 kinase active site was unexpectedly found to drive the selective cellular efficacy of the compounds. Both CHK1 potency and off-target human ether-a-go-go-related gene (hERG) ion channel inhibition were dependent on lipophilicity and basicity in this series. Optimization of CHK1 cellular potency and *in vivo* pharmacokinetic-pharmacodynamic (PK-PD) properties gave a compound with low predicted doses and exposures in humans which mitigated the residual weak *in vitro* hERG inhibition.

## INTRODUCTION

The serine-threonine kinase CHK1 is a critical component of the cellular response to DNA damage, especially the repair of DNA breaks arising during replication or caused by DNA-damaging chemotherapies and ionizing radiation.<sup>1</sup> CHK1 is activated by the upstream kinases ataxia telangiectasia and Rad3-related (ATR), and to a lesser extent ataxia telangiectasia mutated (ATM).<sup>2</sup> CHK1 is phosphorylated on residues S317 and S345 by ATR, and undergoes autophosphorylation on S296.<sup>3</sup> The activated enzyme phosphorylates a range of substrates, including the cell division cycle 25 (CDC25) family of phosphatases that regulate cell cycle

progression, with the result that the cell cycle is halted at checkpoints in Synthesis (S) or Gap 2 (G2) phase.<sup>4</sup> At the same time, CHK1 initiates DNA repair by homologous recombination through signaling to the repair protein RAD51.<sup>5</sup> The cell cycle checkpoints controlled by CHK1 therefore provide an opportunity for repair of the damaged DNA before the replicating cell enters mitosis. If the damage is resolved the checkpoint is released and cell growth and division recommence, while prolonged activation of the checkpoint leads to senescence or cell death.

The DNA damage response (DDR) mediated by ATR-CHK1 provides a mechanism for cancer cells to resist DNA-damaging anti-cancer therapies and is an attractive point of intervention for new treatments.<sup>6</sup> A strong body of evidence shows that inhibition of CHK1 with small molecules, or depletion by ribonucleic acid (RNA) interference, selectively sensitizes tumor cells to genotoxic drugs and ionizing radiation.<sup>7</sup> Normal cells have multiple DNA-damage checkpoints, including the important p53-dependent Gap 1 (G1) phase checkpoint. However, many cancer cells harbor defects in one or more of these checkpoints, for example due to frequent deletion, mutation and loss of function of the tumor suppressor p53, and rely on the S and G2 checkpoints mediated by CHK1 to effect repair of DNA damage.<sup>8</sup>

The potential of CHK1 inhibition as a mono-therapy has been demonstrated in tumor cells with replication stress. These tumors rely on the CHK1-mediated DDR to repair intrinsically high levels of DNA strand breaks, for example arising from increased replication fork stalling in S phase, and include cancers driven by v-myc avian myelocytomatosis viral oncogene homolog (MYC) and v-myc avian myelocytomatosis viral oncogene neuroblastoma derived homolog (MYCN) oncogenes<sup>9,10</sup>, as well as some melanomas and triple-negative breast cancers.<sup>11,12</sup>

There has been substantial activity in developing CHK1 inhibitors for clinical study in combination with various DNA-damaging agents.<sup>7,13</sup> While the first clinical studies have

demonstrated the tolerability of CHK1 inhibition, further progression has often been challenging and development of several agents has been halted after early phase clinical trials. Some of the first generation inhibitors have low selectivity for CHK1, and were developed as intravenous agents. Subsequent to the identification of these compounds, studies showed that maximum potentiation of gemcitabine efficacy in preclinical models was associated with exposure to the CHK1 inhibitor during a window beginning some 24 h after administration of the genotoxic agent.<sup>14,15</sup> Consequently, an oral compound would offer advantages of ease of administration and flexibility of scheduling. In addition, preclinical data on the emerging contexts for CHK1 monotherapy suggests that daily dosing may be needed, for which an oral drug would again be favored. The oral CHK1 inhibitors GDC-0425 and GDC-0575 have been reported in Phase I clinical trials.<sup>16,17</sup> There remains a clear need for highly selective, oral CHK1 inhibitors from different chemical series to advance to clinical studies.

We previously reported the discovery and optimization of the first published selective, oral CHK1 inhibitor (*R*)-3-((1-(dimethylamino)propan-2-yl)oxy)-5-((4-methoxy-5-(1-methyl-1H-pyrazol-4-yl)pyridin-2-yl)amino)pyrazine-2-carbonitrile (**1**)<sup>18</sup> through a scaffold hybridization strategy starting from potent, selective but highly metabolized inhibitor (*R*)-5-((8-chloroisoquinolin-3-yl)amino)-3-((1-(dimethylamino)propan-2-yl)oxy)pyrazine-2-carbonitrile (**2**) and the less potent but metabolically stable 5-((4-aminopyridin-2-yl)amino)pyrazine-2-carbonitrile **3** (Figure 1).<sup>19,20</sup> While effective in preclinical models, compound **1** was suboptimal due to low metabolic stability in human hepatocytes, leading to predictions of poor human pharmacokinetics (PK) and a requirement for high doses. In parallel with the discovery of **1**, we pursued the multi-parameter optimization of the 5-((4-aminopyridin-2-yl)amino)pyrazine-2-carbonitriles based on **3**, described herein, resulting in the identification of the potent and highly

selective, oral CHK1 clinical candidate, (*R*)-5-((4-((morpholin-2-ylmethyl)amino)-5-(trifluoromethyl)pyridin-2-yl)amino)pyrazine-2-carbonitrile (**4**; CCT245737).<sup>21</sup>

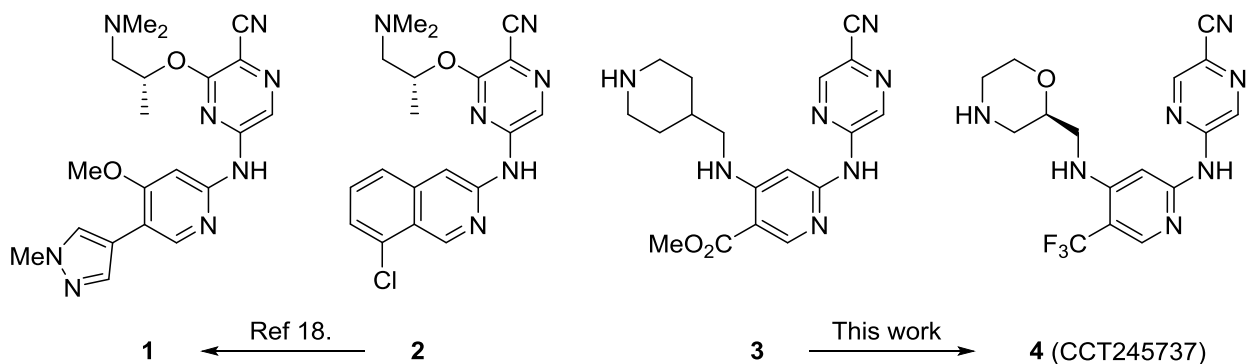


**Figure 1.** Summary of the evolution of the oral inhibitor tool compound **1**<sup>18</sup> and oral clinical development candidate **4**.<sup>21</sup>

## RESULTS AND DISCUSSION

### Assay cascade and target candidate profile

The desired candidate profile was developed based on our experience with compounds **1** and **2**. Potent biochemical inhibition of CHK1 ( $IC_{50} < 10$  nM) was required. We measured CHK1 inhibition using a Dissociation-Enhanced Lanthanide Fluorescent Immunoassay (DELFI) format and also developed a microfluidic assay for CHK1 substrate phosphorylation with a larger dynamic range to accurately assess tight-binding compounds. High selectivity for CHK1 over other kinases was considered essential. In particular, inhibition of the structurally distinct DDR protein, checkpoint kinase 2 (CHK2), has been shown to be detrimental to the potentiation of the cytotoxicity of DNA damaging agents and radiotherapy by CHK1 inhibition.<sup>22</sup> In contrast to *CHEK1*, encoding for the CHK1 protein, the *CHEK2* gene is a tumor susceptibility gene, and

selective inhibition of CHK2 does not sensitize cancer cells to a range of DNA-damaging agents.<sup>23,24</sup> We also monitored compounds for inhibition of the cell cycle regulatory kinase, cyclin dependent kinase 1 (CDK1). Continued cell cycle progression into mitosis is necessary to expose cancer cells to the deleterious effects of enhanced DNA damage through checkpoint abrogation. Inhibition of cell cycle regulatory kinases such as CDK1, itself an indirect downstream target of activated CHK1, would lead to CHK1-independent cell cycle arrest that would confound interpretation of the cellular activity of the compounds. In both cases, we considered biochemical selectivity of >100-fold a minimum requirement. As lipophilic bases present a general risk of ion channel inhibition, we monitored hERG inhibition as a representative and clinically relevant off-target during lead optimization.

Potent and highly selective inhibition of CHK1-dependent effects in human cancer cells was considered essential and we specified an  $IC_{50} < 100$  nM for the abrogation of a CHK1-dependent etoposide-induced G2/M checkpoint in p53-deficient HT29 human colon cancer cells.<sup>20</sup> To measure CHK1 selective effects in cells, the potency for the CHK1-specific checkpoint abrogation was compared with the non-specific anti-proliferative effect of the inhibitors in the same cell line, with a minimum requirement of five-fold cellular selectivity.<sup>20</sup> We used this ratio of cellular effects as an integrated surrogate for kinome-wide or other large scale biochemical profiling of multiple compounds during lead optimization. The growth of HT29 cells is not highly sensitive to selective inhibition of CHK1, thus the ratio of the potency for this CHK1-independent effect to that for the CHK1-dependent checkpoint abrogation informs on the target selectivity of the compounds. Compounds with sufficient cellular potency and selectivity were assessed for their ability to potentiate the cytotoxicity of the DNA-damaging agent gemcitabine in SW620 human colon cancer cells. CHK1 inhibition has been shown to synergize maximally

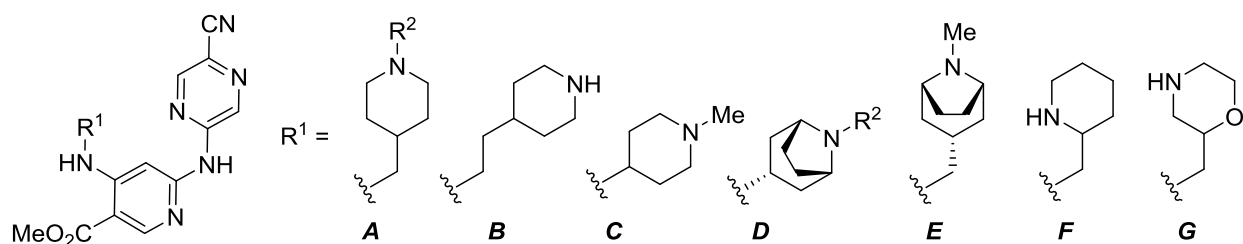
with anti-metabolites such as gemcitabine compared with other classes of DNA-damaging chemotherapies.<sup>25</sup>

Cellular studies of the tool compound **1** had shown that sustained inhibition of CHK1 signaling after administration of the DNA-damaging agent was required for maximal potentiation of the efficacy of the cytotoxic agent.<sup>14</sup> Therefore; compounds with sufficient metabolic stability, plasma concentration and pharmacodynamic (PD) duration of action to give 24 h inhibition of the target following a single oral dose were sought. Inhibition of the autophosphorylation of CHK1 on S296 in HT29 human tumor xenografts was used as a PD measure of target protein engagement.<sup>14</sup>

### **Optimization of *in vitro* and PK properties**

Compound **3** (Table 1) presented an encouraging starting point for realization of the desired clinical candidate profile. While requiring increases in cellular potency and selectivity, the compound showed more than 400-fold selectivity for *in vitro* inhibition of CHK1 over CHK2, and was stable in mouse liver microsomes (MLM) (9% metabolized after 30 min; Table S1, Supporting Information). To improve on **3** we chose to retain the 5-aminopyrazine-2-carbonitrile group, as our extensive structural biology studies to develop the series had shown this group to interact optimally with unique protein-bound water molecules in CHK1, conferring high selectivity over other kinases.<sup>19</sup> Basic substitution at C-4 of the pyridine core was retained to maximize affinity through potential interactions with polar residues in the ribose binding pocket of the CHK1 active site, as we had previously shown for 5-((6-((piperidin-4-ylmethyl)amino)pyrimidin-4-yl)amino)pyrazine-2-carbonitrile (PDB: 2YM7) and other compounds prepared during the identification of **3**.<sup>19</sup>

**Table 1:** *In vitro* properties of selected 4-amino-substituted methyl 6-((5-cyanopyrazin-2-yl)amino)nicotines



No	R <sup>1</sup>	R <sup>2</sup>	CHK1 IC <sub>50</sub> (nM) <sup>a</sup>	CHK2 IC <sub>50</sub> (μM) <sup>b</sup>	Checkpoint abrogation IC <sub>50</sub> (nM) <sup>c</sup>	Cellular selectivity (fold) <sup>d</sup>	hERG (%inhibition @ 10 μM) <sup>e</sup>
3	<i>A</i>	H	21 (±6)	9.6 (±2.4)	825 (±125)	3.8	39
5	<i>B</i>	-	11 (±0.1)	9.8 (±1.3)	440 (±130)	5.1	55
6	<i>A</i>	Me	19 (±1)	-	850 (±450)	4.3	82
7	<i>C</i>	-	2.9 (±0.1)	14 <sup>f</sup>	129 (±62)	4.4	69
8	<i>(s)-D</i>	H	1.0 <sup>f</sup>	11 (±5)	21 <sup>f</sup>	6.2	58
9	<i>D</i> <sup>g</sup>	Me	0.5 <sup>f,h</sup>	2.2 <sup>f</sup>	12 (±6)	7.5	91
10	<i>(s)-E</i>	-	7.0 (±0.3)	-	2500 <sup>f</sup>	6.8	60
11	<i>rac-F</i>	-	56 <sup>b,f</sup>	-	1100 <sup>f</sup>	3.5	42
12	<i>rac-G</i>	-	2.2 (±0.3)	5.0 <sup>f</sup>	310 <sup>f</sup>	3.5	24

<sup>a</sup> Determined in Caliper microfluidic assay, mean (±SD) for n=2. <sup>b</sup> Determined in DELFIA, mean (±SD) for n=2. <sup>c</sup> Abrogation of etoposide-induced G2 checkpoint arrest in HT29 human colon cancer cells, mean (±SD) for n=2. <sup>d</sup> Ratio of antiproliferative GI<sub>50</sub> (measured in duplicate by sulforhodamine B (SRB) assay) to IC<sub>50</sub> for CHK1-mediated abrogation of etoposide-induced G2 checkpoint arrest in HT29 human cancer cells. <sup>e</sup> Inhibition of hERG ion current in HEK cells overexpressing hERG ion channel (PatchExpress, Millipore Inc.), single determination at 10 μM. <sup>f</sup> Single determination. <sup>g</sup> Prepared as a mixture of (3s) and (3r) isomers. <sup>h</sup> Below tight-binding limit of assay.

Initially we examined a range of 4-amino-substituted methyl 6-((5-cyanopyrazin-2-yl)amino)nicotines to determine the scope for replacing the 4-(piperidine-4-methyl) substituent of **3**, with selected examples shown in Table 1. Homologation (**5**) or truncation (**7**) of the linking alkyl chain, and *N*-methylation (**6** and **7**) of the piperidine were tolerated, with increased CHK1 inhibition and cellular potency for **7**. The tropane derivatives **8**, **9** and **10** showed potent inhibition of CHK1 activity ( $IC_{50} < 10$  nM), translating to cellular potency of  $< 100$  nM for **8** and **9** and cellular selectivity exceeding the target threshold of five-fold. The racemic piperidin-2-methyl analogue **11** retained the profile of **3** while the racemic morpholin-2-yl-methyl derivative **12** had enhanced biochemical inhibition compared to the piperidines **3** and **11**, with more potent checkpoint abrogation in cells, but a greater differential between biochemical and cellular activities.

While the increased lipophilicity of the tropane derivatives led to improved potency and cellular selectivity, it was also associated with more potent hERG inhibition, particularly for the *N*-methyl derivative **9**. In contrast, the racemic morpholin-2-yl-methyl derivative **12** delivered enhanced CHK1 affinity with minimal hERG inhibition. Reductions of amine lipophilicity or basicity are documented as strategies for reducing hERG activity.<sup>26</sup> hERG inhibition by a wider group of 4-amino-substituted methyl 6-((5-cyanopyrazin-2-yl)amino)nicotines prepared during this study, including those exemplified in Table 1, showed a correlation with calculated ALogP (Figure 2). Less potent hERG inhibition was more frequently associated with secondary amines with a total of 3 hydrogen bond donors (HBD) in the molecule, as shown by compounds **3**, **11** and **12**, compared to tertiary amines (2 HBD). This indicated that an increased risk of hERG inhibition would be associated with compounds with higher calculated AlogP in this series, but

this would need to be balanced with the potential for improved CHK1 cellular potency and selectivity with more lipophilic amines.

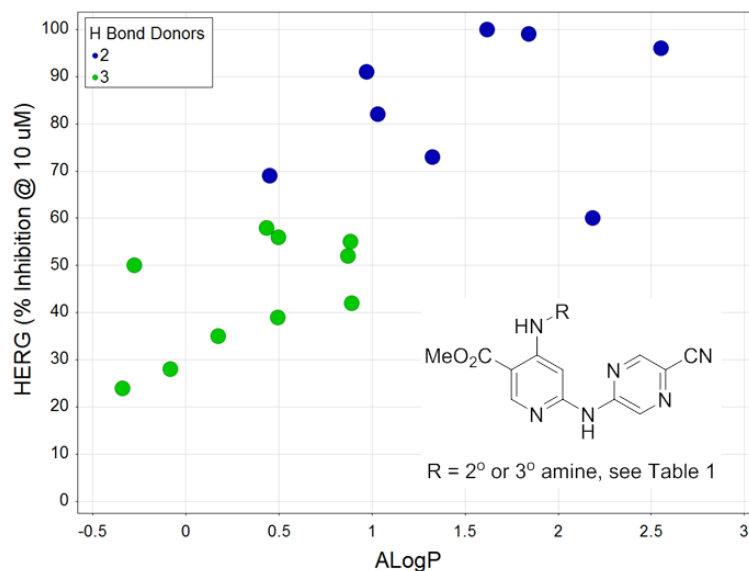


**Figure 2.** Relationship of hERG inhibition to calculated AlogP and HBD count for 4-amino-substituted methyl 6-((5-cyanopyrazin-2-yl)amino)nicotinate including examples specified in Table 1.

During the optimization of the series, selected compounds were screened for metabolic stability in MLM and typically showed <30% metabolism of the parent compound after 30 min (see Table S1, Supporting Information). The mouse PK profiles of the esters **5** and **7** were determined (Table 2). Compound **5** showed moderate oral bioavailability (44%), high volume of distribution, and clearance greater than liver blood flow. *In vivo* clearance was substantially increased for the *N*-methyl piperidine analogue **7** despite similar MLM *in vitro* stability (26% and 28% metabolized after 30 min for **5** and **7**, respectively; Table S1, Supporting Information). A number of methyl ester-substituted analogues in the related 3-alkoxy-5-(pyridin-2-

ylamino)pyrazine-2-carbonitrile scaffold<sup>19</sup> were assessed for stability in human plasma, but no evidence for degradation was seen during a 60 min incubation (data not shown). To efficiently discriminate compounds on the basis of PK performance, we used a limited sampling strategy that compared plasma levels at 1 h and 6 h after i.v. and p.o. dosing<sup>18</sup> to assess compounds *in vivo* with promising *in vitro* potency and selectivity, or with structural features important to the development of structure-activity relationships. This strategy provided a useful ranking of relative oral bioavailability and clearance. Selected compounds were subsequently progressed to full PK determinations (Table 2).

**Table 2:** *In vivo* mouse PK properties of selected compounds following intravenous (i.v.) or oral (p.o.) dosing.

No.	i.v. Dose (mg/kg)	Cl <sup>a</sup> (L/h/kg) <sup>b</sup>	Vss <sup>a</sup> (L/kg) <sup>b</sup>	T <sub>1/2</sub> <sup>a</sup> (h)	p.o. Dose (mg/kg)	F <sup>c</sup> (%)
<b>5</b>	5	8.45	60.5	11	5	44
<b>7</b>	5	54.7	20.2	0.36	5	10
<b>15</b>	5	7.85	7.25	1.6	5	0
<b>25</b>	10	6.75	26.8	4.3	10	53
<b>30</b>	1	0.50	1.15	2.0	5	16
<b>36</b>	10	8.25	10.4	3.8	10	10
<b>38</b>	5	6.35	14.8	2.2	5	68
<b>40</b>	10	6.70	43.9	8.1	10	68
<b>41</b>	10	2.75	10.1	3.4	10	84
<b>4</b>	10	2.65	9.25	2.9	10	105

<sup>a</sup> Parameters from i.v. PK profile. <sup>b</sup> Calculated based on a 20 g mouse body weight. <sup>c</sup> Oral bioavailability.

The crystal structure of **12** bound to CHK1 was determined (PDB: 5F4N, Figure 3). The 2-aminopyridine core formed hydrogen bonds with Glu85 and Cys87 in the kinase hinge region, as seen previously for compounds such as **2** (PDB: 2YM8).<sup>19</sup> The cyanopyrazine was positioned close to the side-chain of Lys38. Importantly, both the nitrile and *N*-4 of the pyrazine ring were positioned to interact with bound water at the entrance to the pocket beyond the gatekeeper residue, one of a network of conserved water molecules resulting from the presence of the unique polar residue Asn59 in this pocket in CHK1 instead of the more common lipophilic side chains. Interactions with these bound waters are a CHK1 selectivity determinant for this and other series of CHK1 inhibitors, including other pyrazines.<sup>27,28</sup> Consistent with this, compounds **3**, **5**, **6**, **7**, **9**, and **12** did not inhibit CDK1 ( $IC_{50} > 10 \mu M$ ).

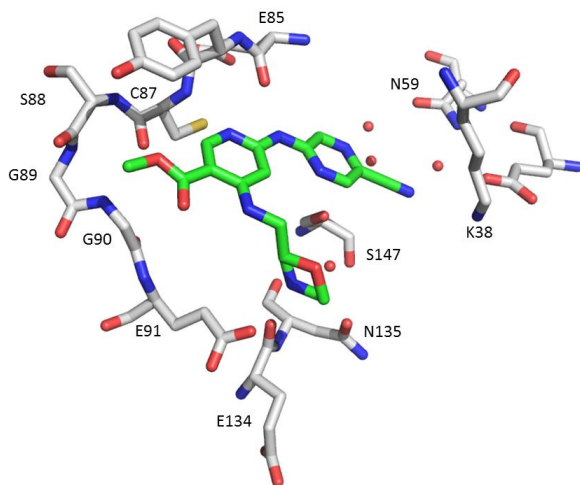


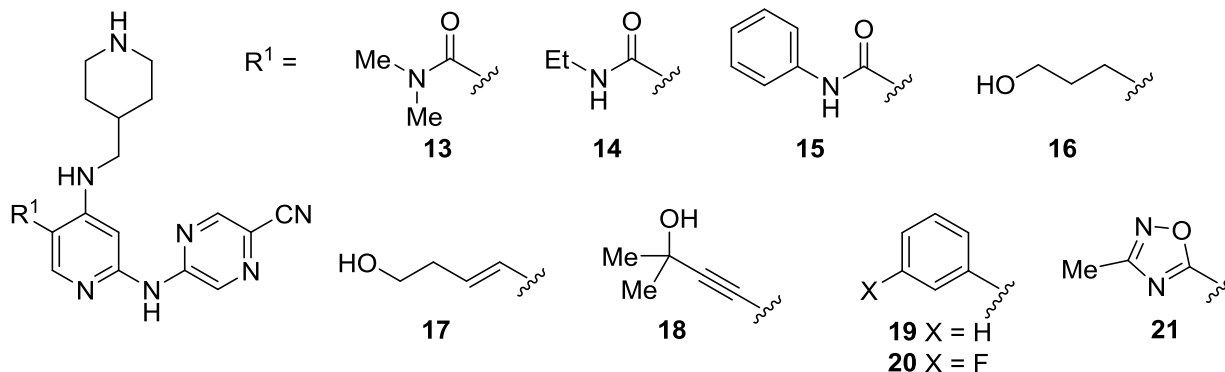
**Figure 3:** Detail of the crystal structure (PDB: 5F4N) showing **12** (green) bound in the CHK1 ATP site with key residues (grey) and water molecules (red spheres) shown.

The crystallographic model indicated only the (*R*)-enantiomer of the morpholine to be bound. The protonated amine of the morpholine engaged in direct interactions with the side-chain of

Glu91 and the main-chain carbonyl of Glu134. In addition, water-mediated interactions to Asn135 and Ser147 were observed, illustrating the rich set of potential contacts available to basic substituents in this region of the kinase and consistent with the generally high CHK1 affinity of the amine variants in Table 1. The morpholine projected towards the main chain of residues Leu15, Gly16 and Glu17 in the P-loop but did not form close contacts. At the entrance to the ATP-pocket, the C-5 methyl ester substituent lay over the selectivity surface formed by Ser88, Gly89 and Gly90. No direct polar interactions of the ester to this moderately hydrophobic surface were observed, suggesting scope for optimization of contacts to the protein. Interestingly, binding of a second molecule of the inhibitor was detected in the crystal structure at a separate hydrophobic site in the N-terminal domain defined by Trp9, Tyr71 and Phe83, however no specific polar interactions of the ligand to the protein were evident and this is unlikely to represent a biologically relevant site of action.

In parallel with variation of the C-4 substituent, investigation of substitution at the C-5 position of **3** was undertaken. The C-5 ester substituent projects towards solvent and was anticipated to provide a handle to optimize *in vitro* activity and allow for modulation of PK properties. A diverse set of substituents from multiple scaffolds has been shown to be capable of binding in this region of CHK1.<sup>27</sup> Compounds were chosen to explore a range of physicochemical properties and the resulting structure-activity relationship is illustrated for specific examples of different substituent types (Table 3).

**Table 3:** *In vitro* properties of selected substituted 5-((4-((piperidin-4-ylmethyl)amino)pyridin-2-yl)amino)pyrazine-2-carbonitriles



No.	CHK1 IC <sub>50</sub> (nM) <sup>a</sup>	Checkpoint abrogation IC <sub>50</sub> (nM) <sup>b</sup>	Cellular selectivity (fold) <sup>c</sup>	hERG (%inhibition@ 10 μM) <sup>d</sup>
<b>13</b>	398 (±48)	-	-	-
<b>14</b>	8.8 (±0.7)	4400 (±400) <sup>e</sup>	5.6	76
<b>15</b>	55 <sup>f,g</sup>	500	7.6	26
<b>16</b>	54 (±4)	>10000	-	-
<b>17</b>	4.7 (±0.8) <sup>f</sup>	4000	4.8	52
<b>18</b>	12 (±1)	3100	4.8	34
<b>19</b>	50 <sup>f,g</sup>	440	5.9	59
<b>20</b>	177 (±8)	600	3.0	-
<b>21</b>	92 (±7)	2500	7.6	64

<sup>a</sup> Determined in Caliper microfluidic assay, mean (±SD) for n=2. <sup>b</sup> Abrogation of etoposide-induced G2 checkpoint arrest in HT29 human colon cancer cells, single determination. <sup>c</sup> Ratio of antiproliferative GI<sub>50</sub> (measured in duplicate by SRB assay) to IC<sub>50</sub> for CHK1-mediated abrogation of etoposide-induced G2 checkpoint arrest in HT29 human cancer cells. <sup>d</sup> Inhibition of hERG ion current in HEK cells overexpressing hERG ion channel (PatchExpress, Millipore Inc.), single determination at 10 μM. <sup>e</sup> Mean (±SD) for n=2. <sup>f</sup> Determined in DELFIA assay. <sup>g</sup> Single determination.

Replacement of the ester with tertiary alkyl amides led to decreased CHK1 inhibition, e.g. **13** (Table 3). Secondary alkyl amides, e.g. **14**, were better tolerated for CHK1 affinity but had poor cellular activity, presumably as a result of the increased polarity and additional HBD compared to **3**. Secondary aryl amides such as **15** offered a better range of CHK1 potencies and retained some cellular activity with increased cellular selectivity over the ester **3**. Compound **15** also showed low hERG inhibition despite the addition of the lipophilic aryl substituent. However, the PK properties of **15** were discouraging, with high clearance and no detectable oral bioavailability (Table 2). Substitution with alkyl, alkenyl and alkynyl groups at C-5 was tolerated for CHK1 inhibition, with a general preference for the unsaturated functionality at C-5 as represented by **17** and **18** compared to **16**. Aryl and heteroaryl substitution also retained CHK1 inhibition, as for example the phenyl **19** and oxadiazole **21** analogues. CHK1 inhibition was sensitive to substitution on the C-5 aryl group, as exemplified by 3-fluorophenyl analogue **20**.

As the inhibitors are ATP-competitive, binding to an active conformation of CHK1 kinase (Figure 3), we expected a decrease in potency in transferring from the CHK1 biochemical assays ([ATP] = 30  $\mu$ M) to cells with high endogenous [ATP]. Esters (see Table 1), aryl amides and heteroaryl or aryl C-5 substituents generally gave the most favorable ratio of potency for G2/M checkpoint abrogation to CHK1 biochemical inhibition (<100-fold).

The SAR described above showed that identifying a clinical candidate CHK1 inhibitor would require balancing the lipophilicity and basicity of the molecules to generate potent CHK1 biochemical inhibition that translated to effective cellular activity and favorable PK properties, while minimizing the risk of ion channel inhibition. We focused on 5-((4-((morpholin-2-ylmethyl)amino)pyridin-2-yl)amino)pyrazine-2-carbonitriles related to morpholine **12**. To help prioritize the selection of C-5 substituents, three *in silico* classification models were generated.

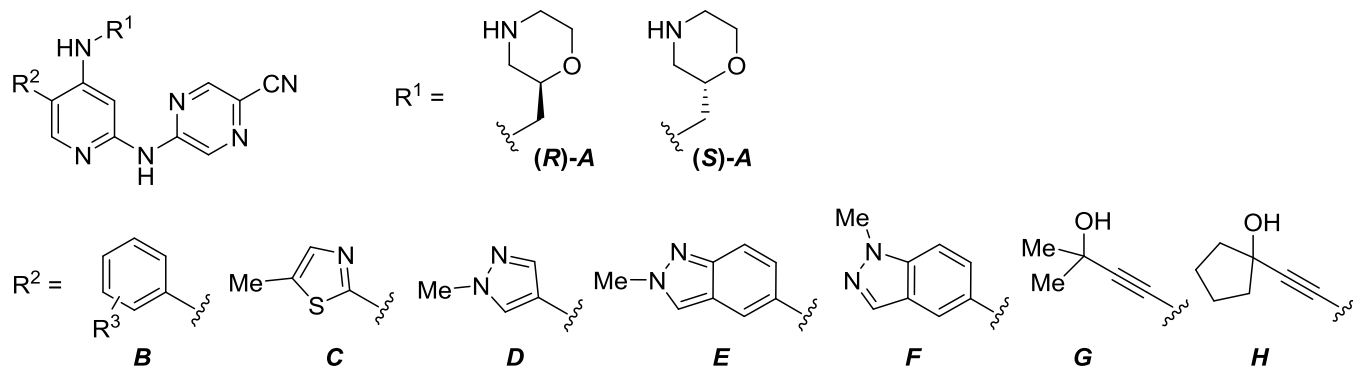
These considered: CHK1 biochemical potency, ratio of CHK1-dependent cellular activity to CHK1 biochemical potency, and inhibition of the hERG ion channel (see Supporting Information). The CHK1 biochemical potency model classified compounds with  $IC_{50} < 25$  nM as active, while the model for the ratio of CHK1-dependent cellular and enzyme activities classed as desirable those compounds that had a less than 50-fold ratio of cellular to enzyme potency. The focus on the translation to cellular potency was driven by the anticipated need for highly potent compounds to achieve a low projected dose in humans. As CHK1 inhibitors will be used as potentiators of conventional cytotoxic chemotherapy, it is important to minimize non-mechanism related toxicity to achieve tolerable combination schedules. Lastly, the hERG model classified compounds as hERG-inactive if their percentage inhibition was less than 40% @ 10  $\mu$ M. Virtual molecules were constructed from two chemotypes that varied in one substituent position (Figure S1, Supporting Information). The first structure, relevant to this work, was based on morpholine **12** with variation of the C-5 substituent. The other structure considered was for the previously described series related to compound **1**.<sup>18</sup> Of the substituents selected to replace the C-5 group in the virtual library, 135 were selected by medicinal chemists and 1514 were extracted from commercially available building blocks. The combinatorial library was enumerated and, after the application of Lipinski Rule-of-Five heuristics, 1649 virtual structures were taken forward for prediction in the three models. The resulting predictions for each of these virtual molecules were used to aid selection of compounds for synthesis, using the normalized probabilities of satisfying the objectives of each of the three models and visual inspection.

Representative 5-((4-((morpholin-2-ylmethyl)amino)pyridin-2-yl)amino)pyrazine-2-carbonitriles related to morpholine **12** are described in Table 4. Replacing the ester of **12** with substituted phenyl groups led to the single enantiomers **22-29**. *In vitro* inhibition of CHK1 was

higher for the morpholine (*R*)-enantiomers (compare **22** vs. **23** and **25** vs. **26**) consistent with the observation of the (*R*)-enantiomer of **12** bound to CHK1 (Figure 3). Compounds **22**, **23**, **25** and **26** were tested for inhibition of CHK2 and retained >100-fold selectivity for CHK1. The cellular profiles of these compounds were similar to **12**, with no improvement in cellular potency except for the 3-fluorophenyl analogue **25**. hERG inhibition was increased over **12** for these lipophilic analogues. Replacing the *C*-5-aryl groups by monocyclic heteroaromatics improved cellular potency, e.g. thiazole **30** and *N*-methyl pyrazole **31**. The (*R*)-enantiomer of the morpholine was again preferred (compare **31** vs. **32**). Combining the polar pyrazole and lipophilic phenyl functionalities in the *N*-methylandazoles **33** and **34** compromised the cellular potency and selectivity compared to the corresponding pyrazole **31**.

The ability of selected compounds to potentiate the efficacy of the cytotoxic drug gemcitabine in p53-deficient SW620 human colon cancer cells was investigated (Table 4). The cell active *C*-5-aryl analogues **25** and **26** had moderate cellular selectivity, and both potentiated the efficacy of gemcitabine. While the thiazole and pyrazole analogues **30-32** strongly potentiated gemcitabine cytotoxicity in cells, the indazoles **33** and **34** surprisingly showed minimal activity. The cellular selectivities of **33** and **34** were reduced compared with other analogues, suggesting that off-target activities may be confounding the CHK1-dependent effects.

**Table 4:** Properties of selected substituted 5-((4-((morpholin-2-ylmethyl)amino)pyridin-2-yl)amino)pyrazine-2-carbonitriles.



No.	R <sup>1</sup>	R <sup>2</sup>	R <sup>3</sup>	CHK1 IC <sub>50</sub> (nM) <sup>a</sup>	Checkpoint abrogation IC <sub>50</sub> (nM) <sup>b</sup>	Cellular selectivity (fold) <sup>c</sup>	Cellular efficacy (fold) <sup>d</sup>	hERG %inhibition (IC <sub>50</sub> , μM) <sup>e</sup>
22	(R)-A	B	4-OMe	6.4 (±0.1)	900	4.3	-	86
23	(S)-A	B	4-OMe	11 <sup>f</sup>	1500	4.5	-	73
24	(S)-A	B	4-F	25 (±1)	800	6	-	64
25	(R)-A	B	3-F	6.4 (±0.6)	120	5.8	7.9	71 (8.8)
26	(S)-A	B	3-F	17 (±4)	390	10	4.8	71 (8.1)
27	(R)-A	B	3-Cl	5.2 (±1)	600	2.2	-	63
28	(R)-A	B	3,4-F <sub>2</sub>	14 (±0.5)	-	-	-	-
29	(R)-A	B	3,5-F <sub>2</sub>	12 (±2)	630	6.7	7.6	38
30	(R)-A	C	-	0.5 <sup>f,g</sup>	13	6.3	8.2	38 (56)
31	(R)-A	D	-	0.9 <sup>g</sup> (±0.1)	60	11	7.4	67 (8.6)
32	(S)-A	D	-	3.2 (±0.8)	400	3.5	8	26 (22)
33	(R)-A	E	-	8.5 (±1)	1000	4.2	1.9	51 (16)
34	(R)-A	F	-	4.6 (±0.4)	240	3.8	1.9	69
35	(R)-A	G	-	0.5 <sup>f,g</sup>	280	4.3	-	39

<b>36</b>	( <i>S</i> )- <i>A</i>	<i>G</i>	-	2.2 ( $\pm$ 0.4)	180	9.2	8.6	28 (26)
<b>37</b>	( <i>S</i> )- <i>A</i>	<i>H</i>	-	2.1 ( $\pm$ 0.1)	72	12	5.6	47 (16)
<b>38</b>	( <i>S</i> )- <i>A</i>	-C $\equiv$ CH	-	5.2 ( $\pm$ 0.8)	100	29	22	68 (8.2)
<b>39</b>	<i>rac</i> -( <i>A</i> )	-C $\equiv$ N	-	23 ( $\pm$ 3)	1600	24	-	8
<b>40</b>	( <i>S</i> )- <i>A</i>	- <i>cyc</i> -Pr	-	7.4 ( $\pm$ 1.4)	100	9	7.3	79 (6.6)
<b>4</b>	( <i>R</i> )- <i>A</i>	-CF <sub>3</sub>	-	1.3 ( $\pm$ 0.4)	30 ( $\pm$ 11) <sup>h</sup>	23	17	76 (6.2)
<b>41</b>	( <i>R</i> )- <i>A</i>	-Cl	-	1.9 ( $\pm$ 0.8)	157 ( $\pm$ 37) <sup>h</sup>	14	18	83 (6.1)
<b>42</b>	( <i>R</i> )- <i>A</i>	-F	-	14 ( $\pm$ 1)	-	-	-	39

<sup>a</sup> Determined in Caliper microfluidic assay, mean ( $\pm$ SD) for  $n \geq 2$ . <sup>b</sup> Abrogation of etoposide-induced G2 checkpoint arrest in HT29 human colon cancer cells, single determination. <sup>c</sup> Ratio of antiproliferative GI<sub>50</sub> (measured in duplicate by SRB assay) to IC<sub>50</sub> for CHK1-mediated abrogation of etoposide-induced G2 checkpoint arrest in HT29 human cancer cells. <sup>d</sup> Fold-potential of gemcitabine cytotoxicity in SW620 human colon cancer cells, determined as the ratio of GI<sub>50</sub> (test compound)/GI<sub>50</sub> (test compound + fixed dose Gemcitabine) in an SRB assay (ref 19). <sup>e</sup> Inhibition of hERG ion current in HEK cells overexpressing hERG ion channel (PatchExpress, Millipore Inc.), single determination at test concentration of 10  $\mu$ M, IC<sub>50</sub> determination ( $n=1$ ) in parentheses. <sup>f</sup> Single determination in DELFIA assay. <sup>g</sup> Below tight-binding limit of assay. <sup>h</sup> Mean ( $\pm$ SD),  $n \geq 3$ .

Key *C*-5-aryl and *C*-5-heteroaryl analogues were screened for *in vivo* PK properties (Table 2). The 3-fluorophenyl derivative **25** showed a similar *in vivo* clearance and bioavailability to the ester **5**. The thiazole **30** had low *in vivo* clearance but poor oral bioavailability, presumed to be due to poor absorption and consistent with the 20-fold lower volume of distribution for this compound. The potent pyrazole **31** was assessed *in vivo* by limited sampling PK, where a drop in plasma levels at 6 h to <20% of those at 1 h indicated a high clearance relative to **5** and the compound was not profiled further.

In tandem with (hetero)aryl groups, non-aryl *C*-5-substituents were prepared in the 5-((4-((morpholin-2-ylmethyl)amino)pyridin-2-yl)amino)pyrazine-2-carbonitrile series (Table 4). The 2-methylbut-3-yn-2-ols **35** and **36** potently inhibited CHK1 with cellular activity and selectivity

similar to the aryl substituted analogues. The 1-ethynylcyclopentan-1-ol analogue **37** increased potency *in vitro* and in cells. Both **36** and **37** potentiated the efficacy of gemcitabine in SW620 cells but the PK profile of **36** showed high clearance and low oral bioavailability (Table 2).

The terminal alkyne derivative **38** was found to retain cellular activity, and to have exceptionally high cellular selectivity compared to other compounds in this series. The potentiation of the anti-proliferative effects of gemcitabine by the alkyne **38** was also increased. The nitrile analogue **39** gave very high cellular selectivity but with reduced biochemical and cellular potency. Other small substituents at *C*-5 were investigated (Table 4) and the structure-activity relationship for the potentiation of gemcitabine cytotoxicity in SW620 human colon cancer cells revealed an inverse correlation to the size of the *C*-5 substituent, as measured by molecular weight or heavy atom count (Figure 4). The cellular selectivity for CHK1-mediated effects followed a similar trend. The crystal structure of **12** bound to CHK1 (Figure 3) indicated that substitution at the *C*-5-position would become directed into solvent with increasing size rather than making contacts with the CHK1 protein. We therefore speculate that the structure-activity relationships for high cellular efficacy and selectivity reflected confounding off-target interactions, possibly one or more kinases, that increased with increasing size of the *C*-5-substituent and interfered with the ability of the CHK1 inhibitor to potentiate genotoxic efficacy.

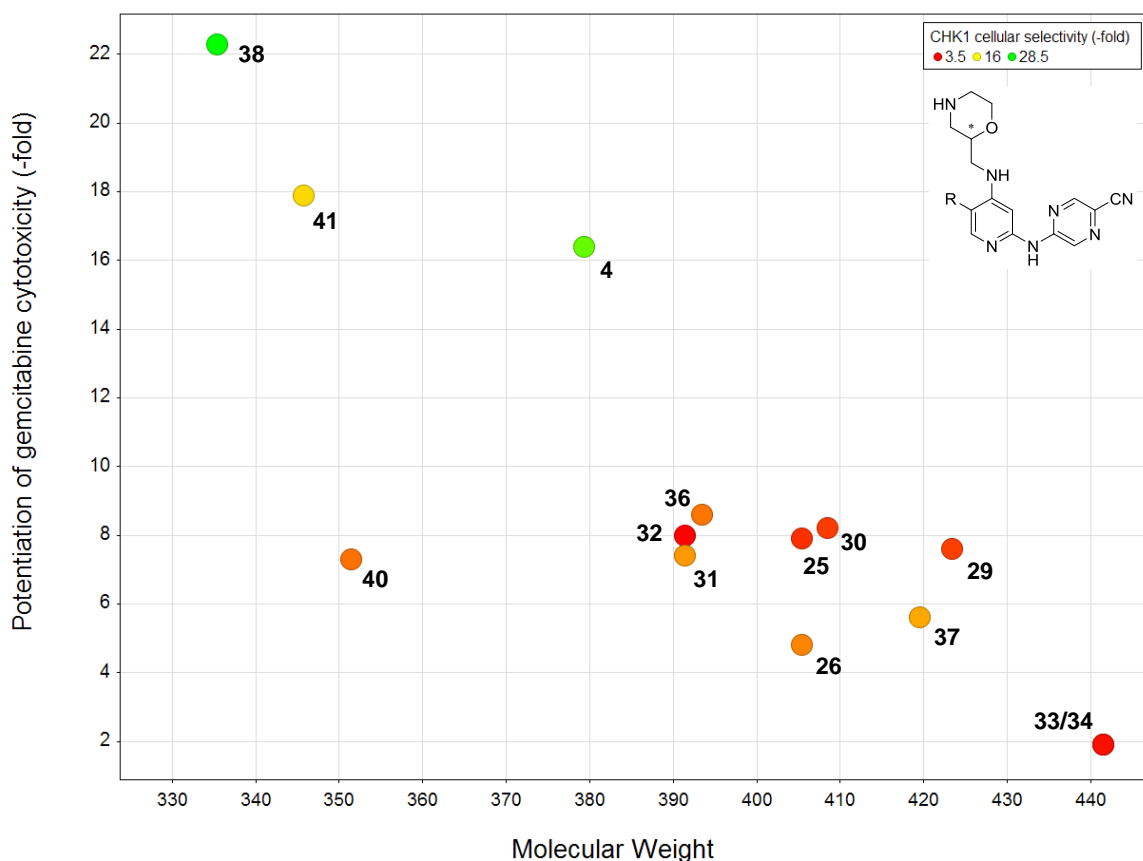


**Figure 4.** Relationship of efficacy and selectivity in SW620 colon cancer cells to molecular weight for 5-((4-((morpholin-2-ylmethyl)amino)pyridin-2-yl)amino)pyrazine-2-carbonitriles with *C*-5 substituents of various sizes, exemplified in Table 4. Points are color-coded by CHK1 cellular selectivity (red – low, green – high) and labelled with compound identifiers.

Among the smaller substituents investigated at *C*-5, the cyclopropyl analogue **40** maintained potency but with decreased cellular selectivity and efficacy. In contrast, both the trifluoromethyl-**4** and chloro-derivative **41** had excellent potency and cellular selectivity, and were strong potentiators of gemcitabine efficacy in cancer cells. Consistent with the cellular profile, these compounds were more than 1000-fold selective for CHK1 over CHK2 and CDK1. The

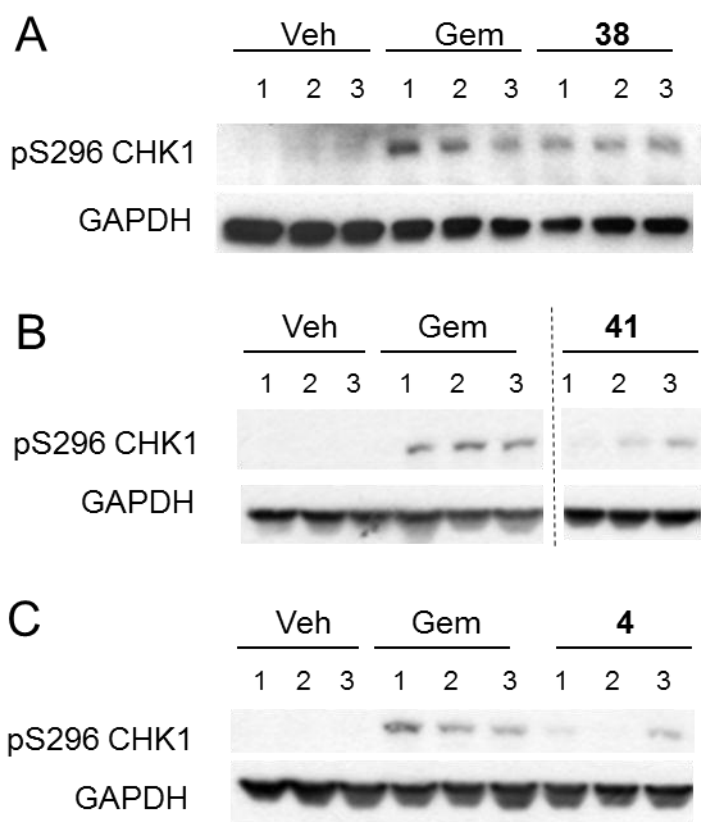
importance of the presence of a suitable C-5 substituent for CHK1 affinity was shown by the fluoro analogue **42** which was ten-fold less potent than **4**. Although more potent and efficacious in cells, the smaller and more lipophilic C-5 substituents were associated with micromolar hERG inhibition. This was balanced by an improvement in PK properties. Thus, the terminal alkyne **38** and cyclopropane **40** had improved oral bioavailability compared to **5**, while both the trifluoromethyl **4** and chloro analogue **41** had substantially reduced *in vivo* clearance and increased oral bioavailability (Table 2). Inhibition of CYP450 enzymes was determined for selected analogues, and compounds **36**, **38**, **40**, **41** and **4** all showed  $IC_{50} > 10 \mu M$  against the 6 isoforms tested (1A2, 2A6, 2C9, 2C19, 2D6, 3A4).

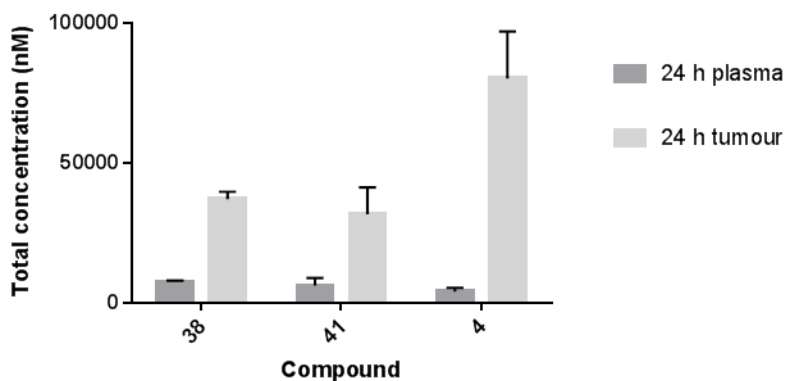
### **Optimization of *in vivo* target engagement and efficacy**

In parallel with the optimization of *in vitro* and PK properties, the PD properties of this series of CHK1 inhibitors were assessed *in vivo*. Following DNA damage, CHK1 is activated through phosphorylation on Ser317 and Ser345 by the upstream kinase ATR, and undergoes autophosphorylation on Ser296. We therefore chose inhibition of the gemcitabine-induced CHK1 Ser296 autophosphorylation as a direct PD biomarker of CHK1 inhibition *in vivo*. Selected compounds with moderate to good oral bioavailability, high cellular selectivity and gemcitabine-potentiating efficacy were assessed for tolerability in mice when administered in combination with gemcitabine (60 mg/kg i.v.). The compounds were then tested at the maximum tolerated combination dose for their ability to inhibit gemcitabine-induced pSer296 CHK1 in SW620 human colon cancer xenografts. It has been shown that maximum potentiation of genotoxic efficacy in cells and *in vivo* requires sustained inhibition of CHK1 signaling to prevent effective tumor cell DNA repair, and inhibition of CHK1 for at least 24 – 48 h following

administration may be desirable.<sup>14,15</sup> We therefore sought compounds showing robust pSer296 inhibition up to 24 h following a single oral dose.

The dose of compound **25** (80 mg/kg) was restricted by toxicity, although a partial inhibition of the CHK1 pSer296 signal was seen at 6 h (data not shown). In contrast, single doses of compounds **38** (300 mg/kg), **41** (300 mg/kg), and **4** (300 mg/kg) were very well tolerated. Compound **38** inhibited the gemcitabine-induced autophosphorylation of CHK1 at 6 h (not shown), but CHK1 kinase activity had recovered by 24 h (Figure 5A). In contrast, the two compounds **41** and **4** inhibited gemcitabine-induced pS296 CHK1 for up to 24 h (Figure 5B, C).



**D**

**Figure 5:** Inhibition of gemcitabine (60 mg/kg i.v.)-induced pSer296 CHK1 autophosphorylation at 24 h by 300 mg/kg p.o. of A) **38**, B) **41** and C) **4** in SW620 human colon cancer xenografts. Dashed line indicates where western blot image has been cut. D) Total inhibitor concentrations of **38**, **41** and **4** in plasma and SW620 tumor xenografts at 24 h after a single 300 mg/kg p.o. dose (mean±SD, n=3).

Inhibitor concentrations at 24 h were measured in plasma and the tumor xenografts (Figure 5D). Plasma levels of between 4 – 8  $\mu$ M were seen for **38**, **41** and **4**. Similar levels of **38** were observed despite the higher clearance of this compound compared with **41** and **4** (Table 2). Distribution to tumor tissue was seen for all compounds, with **4** achieving the highest tumor concentration.

The antitumor efficacies of **41** and **4** were investigated in combination with gemcitabine in HT29 human colon cancer xenografts. The dosing schedule was selected based on our previous studies of the oral CHK1 tool compound **1**<sup>14</sup> and involved the administration of two doses of the CHK1 inhibitors at 24 and 48 h after gemcitabine (100 mg/kg i.v.) in each of three, weekly treatment cycles. Compounds **41** and **4** were dosed at their maximum tolerated dose (MTD) (150

mg.kg p.o.) for this schedule in the xenograft tumor model (Figure 6). Both compounds were well tolerated in combination with no significant decrease in body weight. A strong potentiation of the anti-tumor effect of gemcitabine was seen, consistent with the cell-based studies (Table 4), with minimal effects of the CHK1 inhibitors alone in this model. At these doses, tumor regressions were observed in 83% (41) and 100% (4) of the combination-treated cohorts at day 17 immediately following completion of the final treatment cycle.

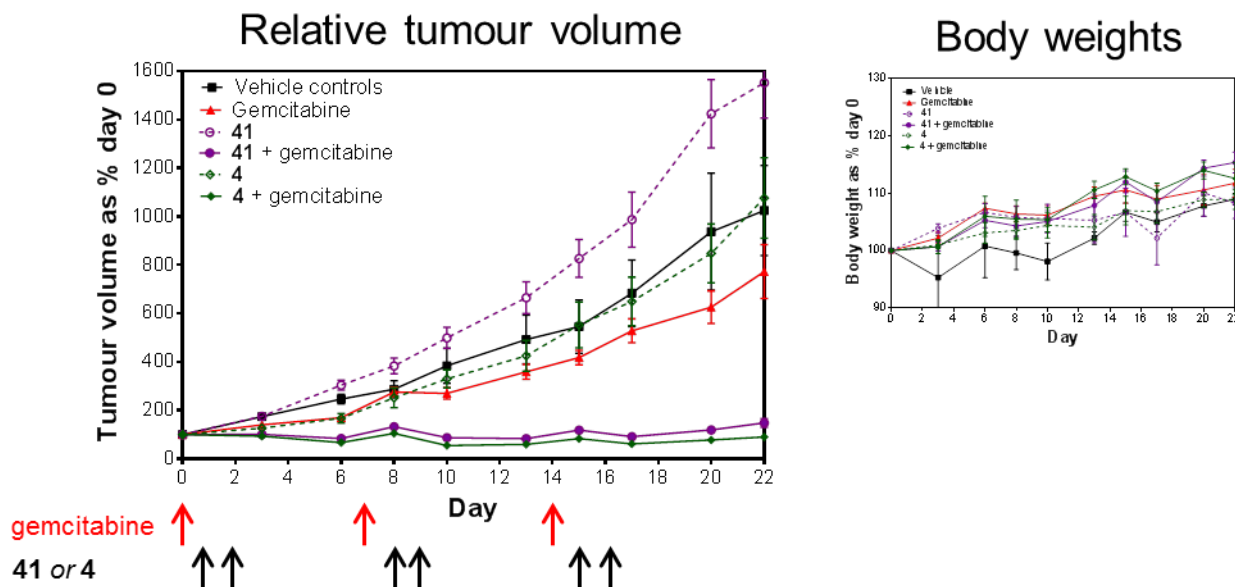


**Figure 6:** Anti-tumor efficacies of 41 (150 mg/kg p.o.) and 4 (150 mg/kg p.o.) in combination with gemcitabine (100 mg/kg i.v.) in HT29 colon cancer xenografts. The CHK1 inhibitors were administered as suspensions in DMSO-Tween80-PEG400-water (0.05:0.2:0.65:0.1) 24 and 48 h after gemcitabine in each of three weekly treatment cycles. Inset: body weights of cohorts as described in main figure. N=4-6 per cohort.

The *in vitro* and *in vivo* PK properties of **41** and **4** were investigated further (Table 5). Both compounds had low oral bioavailability in rats. Although both were high clearance compounds, **4** had a lower clearance than **41**. Pleasingly, determination of the intrinsic clearance (CL<sub>int</sub>) in hepatocytes showed both compounds were substantially more stable in human hepatocytes than mouse, and **4** was more stable in human than rat and dog hepatocytes. In particular, **4** had a favorable low human hepatocyte CL<sub>int</sub>. Predictions of human clearance were made using physiological-based PK (PBPK) modelling<sup>29</sup> and suggested that **4** would have a clearance in humans of 6% liver blood flow.

**Table 5:** Additional *in vivo* and *in vitro* PK data for **41** and **4**.

		<b>41</b>	<b>4</b>
Rat PK	CL (L/h/kg)	5.17	3.50
	V <sub>ss</sub> (L/kg)	7.45	4.60
	F (%)	22	38
Hepatocyte CL <sub>int</sub> ( $\mu\text{L}/\text{min}/10^6$ cells) <sup>a</sup>	Mouse <sup>b</sup>	22.1 ( $\pm 2.6$ )	25.7 ( $\pm 3.4$ )
	Rat	n.d <sup>c</sup>	43.4 ( $\pm 9.96$ )
	Dog	n.d <sup>c</sup>	55.0 ( $\pm 2.1$ )
	Human <sup>d</sup>	4.82 ( $\pm 0.91$ )	2.72 ( $\pm 0.61$ )

<sup>a</sup> Determined at Cyprotex. Incubations at 3  $\mu\text{M}$ . Mean ( $\pm\text{SE}$ ) <sup>b</sup> Incubations in male CD-1 mouse hepatocytes. <sup>c</sup> not determined. <sup>d</sup> Incubations in mixed gender human hepatocytes.

#### ***In vitro* and *in vivo* profile of compound 4**

Compound **4** was further profiled *in vitro* and *in vivo*. The solubility of **4** in pure water was 0.09 mg mL<sup>-1</sup>, rising to 1.5 mg mL<sup>-1</sup> in pH 6.5 phosphate buffer, consistent with the moderate basicity (pK<sub>a</sub> = 7.87  $\pm$  0.07)<sup>30</sup> and lipophilicity (LogD<sub>7.4</sub> = 1.47  $\pm$  0.04)<sup>30</sup> and indicating good

prospects for formulation as a salt. Compound **4** showed passive permeability across a CaCo2 cell monolayer ( $P_e = 25 \times 10^{-6} \text{ cm s}^{-1}$ ). The plasma protein binding of **4** was moderate (mouse  $F_u = 0.19$ ; human  $F_u = 0.21$ , measured using dialysis with pH control). No change in the metabolic stability of **4** was observed in human liver microsomes in the presence and absence of glutathione, indicating that **4** does not undergo metabolic activation. While some electron-deficient heterocyclic nitriles have been reported to be chemically reactive under physiological conditions,<sup>31</sup> we speculate that the balanced electronic donor-acceptor substitution pattern of the 5-aminopyrazine-2-carbonitrile prevents this reactivity. Compound **4** was not metabolized by human aldehyde oxidase.

The kinome selectivity of **4** was assessed against a panel of 124 representative kinases in substrate phosphorylation assays ( $[\text{ATP}] = K_{m,\text{ATP}}$ ).<sup>32</sup> Compound **4** showed <50% inhibition at 10  $\mu\text{M}$  for 85/121 kinases, representing a selectivity for CHK1 inhibition of >5000-fold over these enzymes, while 12/124 (including CHK1) showed >80% inhibition at 10  $\mu\text{M}$  (Table S2, Supporting Information). The activity of these enzymes, along with the potential off-targets CDK1/2 and 5'-AMP-activated protein kinase (AMPK)<sup>33</sup> were titrated (Table S3, Supporting Information). Sub-micromolar activity was identified for seven kinases in this panel, with **4** showing 100-fold selectivity for CHK1 over the most potent off-target kinase activity identified (mitogen-activated protein kinase 15, ERK8) and more than 200-fold selectivity for CHK1 over other kinases tested. These data confirmed the expectation of high CHK1 selectivity from the cellular selectivity of **4**. While medium-throughput whole-kinome profiling during lead optimization is feasible, interpretation of the functional relevance of off-target binding assays remains difficult.<sup>34</sup> Our experience with this inhibitor series shows that appropriate cell-based

mechanistic assays can drive compounds towards high kinome selectivity based on an integrative assessment of on- vs. off-target outcomes in cancer cell lines.

The ability of compound **4** to potentiate the anti-cancer efficacy of DNA-damaging agents was determined in a wider range of cancer cell lines (Supporting Information, Table S4).<sup>21</sup> Potentiation of the efficacy of the anti-metabolite gemcitabine (8 – 23-fold) was significantly greater than that for SN38 (1.8 – 3-fold), the active metabolite of the clinical topoisomerase 1 inhibitor irinotecan. Importantly, in addition to efficacy in colon cancer cell lines, compound **4** strongly potentiated gemcitabine efficacy in non-small cell lung cancer (NSCLC) and pancreatic cancer cell lines. These represent clinical indications where gemcitabine is part of current chemotherapy regimens, and where tumors have a high frequency of p53 mutation or loss-of-function.<sup>35,36</sup> Compromise of the p53-dependent DDR checkpoint may enhance the effectiveness of CHK1 inhibition in combination with genotoxic agents.<sup>7</sup> The inhibition of CHK1 and anti-tumor efficacy of **4** was confirmed in NSCLC and pancreatic cancer tumor xenografts. In particular, **4** potentiated the efficacy of a gemcitabine and carboplatin combination in RAS mutant Calu6 human NSCLC xenografts.<sup>21</sup> *In vivo* efficacy in combination with gemcitabine was further demonstrated in the KPC1 genetically engineered mouse model (GEMM) of p53- and V-Ki-ras2 Kirsten rat sarcoma viral oncogene homolog (KRAS)-deficient pancreatic ductal adenocarcinoma.<sup>37</sup> In cells derived from this model, **4** potentiated the anti-proliferative effect of gemcitabine 18-fold *in vitro*. Allografts from established KPC1 mouse tumors were grown subcutaneously in female NCr athymic mice, and treated with gemcitabine and three dose levels of **4** using the schedule developed during lead optimization. Some single agent efficacy of the highest dose of CHK1 inhibitor was observed in this model in addition to dose-dependent potentiation of gemcitabine efficacy (Figure 7).

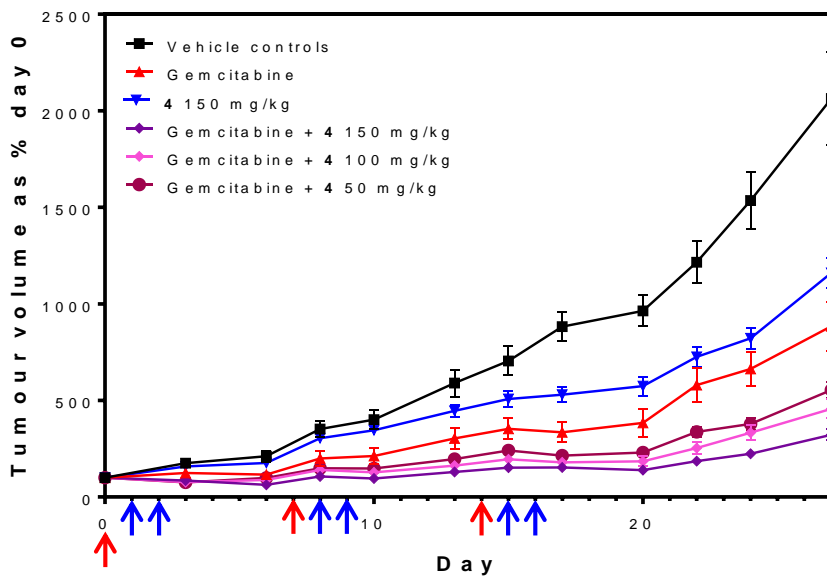


**Figure 7:** **4** (150 mg/kg p.o.) potentiates the tumor growth delay of gemcitabine in allograft KPC1 p53- and KRAS-deficient mouse pancreatic adenocarcinomas.<sup>37</sup> N=8 per cohort. Red arrow = gemcitabine dosed; blue arrow = **4** dosed.

Single agent CHK1 inhibition has recently been identified as a potential therapeutic strategy for MYC-driven tumors that rely on the CHK1-mediated DDR pathway as a result of replication stress.<sup>9,10</sup> We therefore assessed the efficacy of compound **4** *in vivo* in a GEMM of pediatric MYCN-driven neuroblastoma.<sup>38</sup> After treatment for 7 days with compound **4** (150 mg/kg p.o. UID), the weights of excised abdominal tumors were reduced compared with vehicle treated cohorts (T/C = 13%) and an individual mouse assessed by magnetic resonance imaging (MRI)<sup>39</sup> before and after dosing of **4** showed 85% reduction in the pre-treatment tumor volume (Figure 8). Single agent efficacy of **4** was also demonstrated in an E $\mu$ -Myc driven mouse model of B-cell lymphoma.<sup>21</sup>

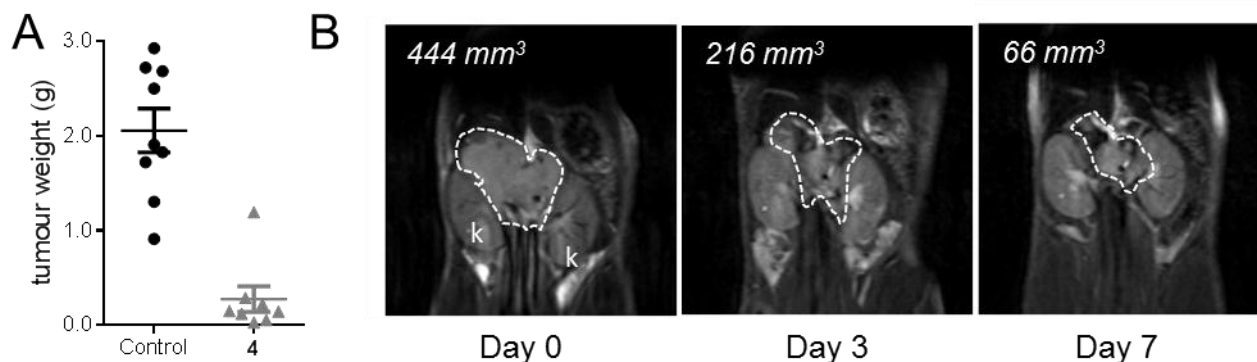


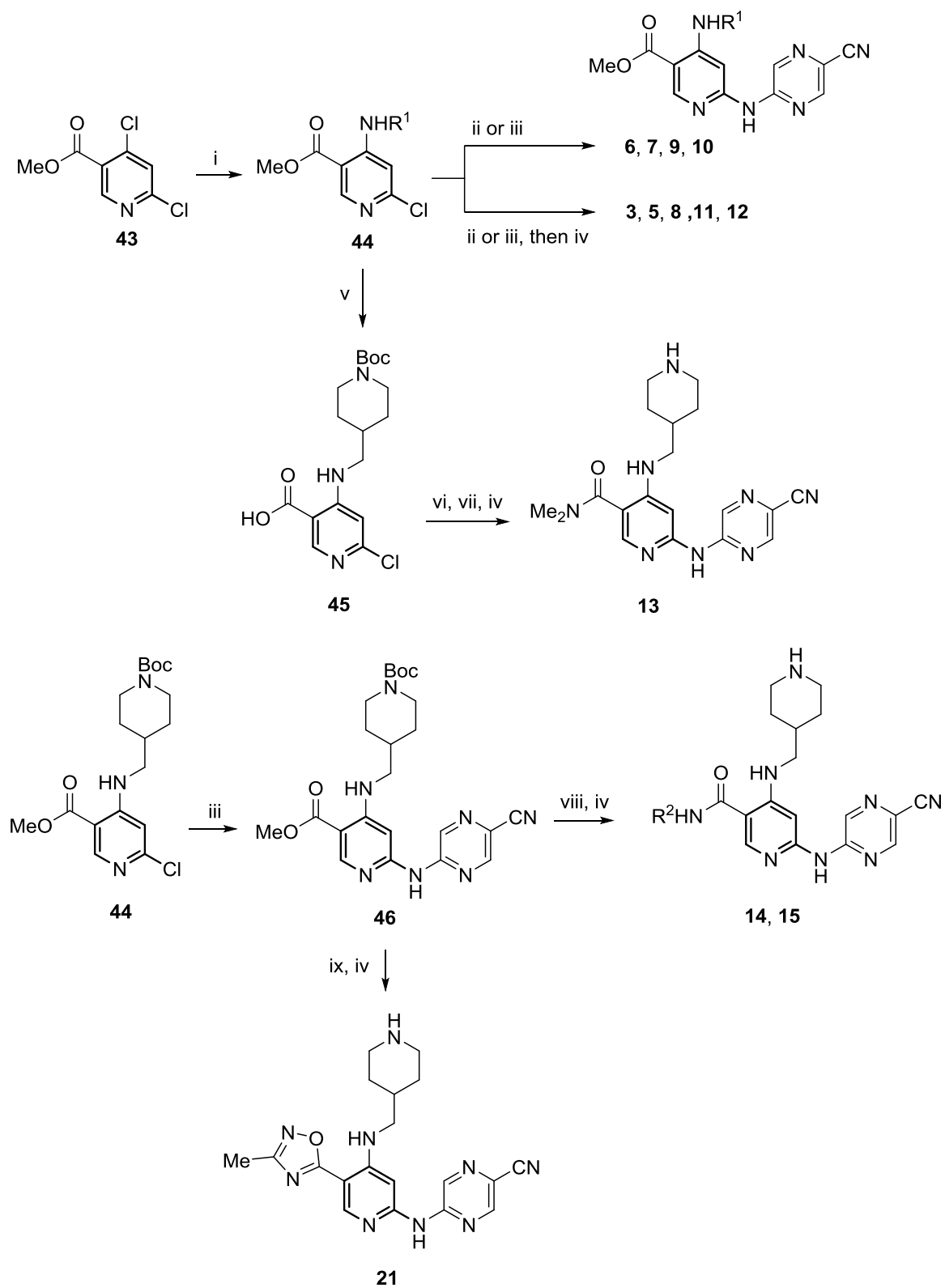
**Figure 8:** **4** (150 mg/kg p.o. UID for 7 d) inhibits tumor growth in the TH-MYCN GEMM of neuroblastoma.<sup>38</sup> A) Comparison of tumor weights for vehicle- and compound-treated cohorts (Mean  $\pm$  SEM, n=8); B) Pre- and post-treatment T<sub>2</sub>-weighted MRI<sup>39</sup> assessment of an abdominal tumor in a single mouse treated with **4**. k = kidney

Dose titration of **4** in combination with gemcitabine (100 mg/kg i.v.) was carried out in HT29 colon cancer xenografts to establish *in vivo* PK-PD relationships and determine a minimum effective dose in this preclinical tumor model. Compound **4** showed an increase in plasma and tumor concentrations between 3 – 100 mg/kg p.o.<sup>21</sup> Modulation of the pSer296 CHK1 autophosphorylation was assessed by western blot from tumor lysates at 24 h after a single dose of **4**, administered 24 h after gemcitabine. Inhibition of pSer296 CHK1 at this time point was observed from 12.5 – 100 mg/kg dose of **4** with no effect for lower doses. Dose-dependent potentiation of gemcitabine efficacy in this model was also observed from doses of 12.5 mg/kg upwards.<sup>21</sup> Calculation of the plasma free drug levels of **4** from the PD dose-titration suggested that complete CHK1 inhibition for 24 h after dosing of **4** was associated with achieving free drug levels of at least 15 nM at 24 h. Single species scaling from mouse<sup>40</sup> and PBPK methods using Simcyp with limited and full simulations were used to predict human clearance and a dose

equivalent to the minimum effective dose of 12.5 mg/kg in mice. Both methods predicted that **4** would show CHK1-dependent effects below 1 mg/kg in humans. For example, the simulated PK profile for a 25 mg total dose in humans predicted a plasma  $C_{\max, \text{free}}$  of *ca.* 70 nM and  $C_{24\text{h}, \text{free}}$  of *ca.* 30 nM, suggesting an acceptable window over the *in vitro* potential for hERG inhibition existed at doses predicted to give free concentrations exceeding those relevant to preclinical biological activity in the human tumor model. Further profiling of cardiac ion channel inhibition was conducted, and **4** showed no inhibition ( $IC_{50} > 10 \mu\text{M}$ ) for seven other K, Ca and Na ion channels (Table S5, Supporting Information).<sup>41</sup> The therapeutic window over potential cardiovascular effects was confirmed by an *in vivo* cardiovascular pharmacology study (data not shown). Compound **4** was selected for progression to preclinical development.

**Chemistry.** General procedures were developed for the synthesis of the C-4 amino-substituted methyl 6-((5-cyanopyrazin-2-yl)amino)nicotinate **3** and **5-12** (Scheme 1). Methyl 4,6-dichloronicotinate (**43**) underwent selective  $S_NAr$  reaction with a range of amines to give the methyl 4-amino-6-chloronicotinate derivatives (**44**). The substituted pyrazine was introduced by Buchwald couplings of the chlorides **44** with 5-aminopyrazine-2-carbonitrile. The majority of compounds were prepared using tris(dibenzylideneacetone)dipalladium(0) and xantphos as the catalyst precursors and cesium carbonate as the base. When these conditions gave poor yields, we found that using tris(dibenzylideneacetone)dipalladium(0), 2,2'-bis(diphenylphosphino)-1,1'-binaphthyl (BINAP) and sodium *tert*-butoxide was successful. Deprotection of *N-tert*-butyloxycarbonyl (*N*-Boc) groups with trifluoroacetic acid was applied where required to generate the test compounds.

**Scheme 1.** Preparation of compounds **3**, **5-15** and **21**.<sup>a</sup>



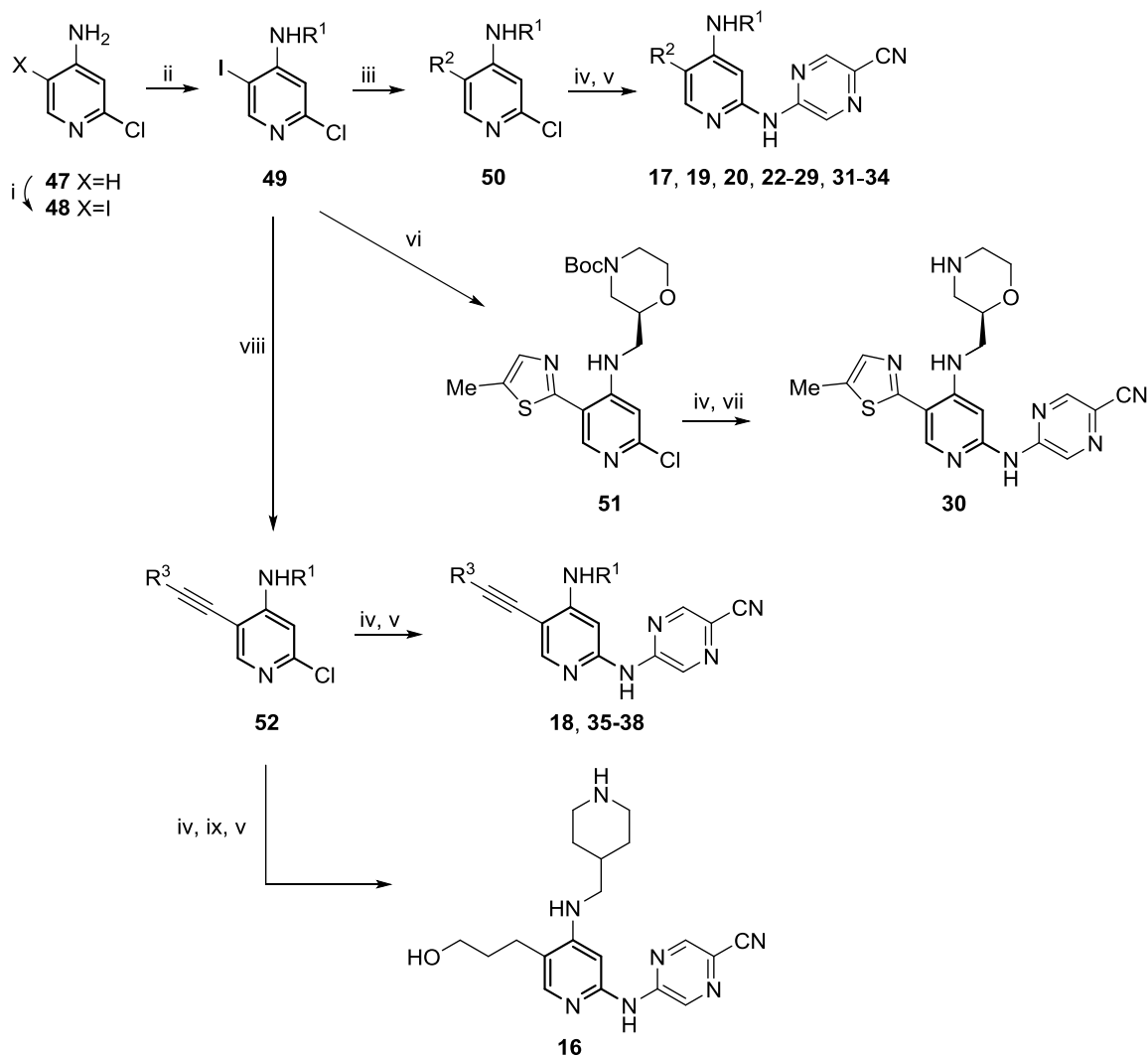
<sup>a</sup> Reagents and conditions: (i) R<sup>1</sup>NH<sub>2</sub>, Et<sub>3</sub>N, <sup>t</sup>BuOH, 120 °C (microwave irradiation), 1.5 h; (ii) 5-aminopyrazine-2-carbonitrile, Pd<sub>2</sub>(dba)<sub>3</sub>, BINAP, NaO<sup>t</sup>Bu, toluene, 130 °C (microwave irradiation), 30 min; (iii) 5-aminopyrazine-2-carbonitrile, Pd<sub>2</sub>(dba)<sub>3</sub>, xantphos, Cs<sub>2</sub>CO<sub>3</sub>, toluene, 130 °C (microwave irradiation), 30 min; (iv) CF<sub>3</sub>CO<sub>2</sub>H, CH<sub>2</sub>Cl<sub>2</sub>, r.t.; (v) NaOH, H<sub>2</sub>O, MeOH, r.t. 3 h; (vi) MeNH<sub>2</sub> (2M, THF), HATU, <sup>i</sup>Pr<sub>2</sub>NEt, DMF, r.t., 18 h; (vii) 5-aminopyrazine-2-carbonitrile, Pd<sub>2</sub>(dba)<sub>3</sub>, xantphos, Cs<sub>2</sub>CO<sub>3</sub>, toluene/DMF (1:1), 130 °C (microwave irradiation), 120 min; (viii) (a) LiOH, H<sub>2</sub>O, <sup>t</sup>BuOH, r.t. 4 d, (b) R<sup>2</sup>NH<sub>2</sub>, TBTU, r.t., 18 h; (ix) (a) LiI, pyridine, 150 °C (microwave irradiation), 2.5 h, (b) *N*'-hydroxyacetimidamide, HATU, <sup>i</sup>Pr<sub>2</sub>NEt, DMF, r.t. 18 h, (c) pyridine, 120 °C (microwave irradiation), 1 h.

The above procedures were adapted for the synthesis of the *C*-5 amide substituted analogues **13-15** and the *C*-5 1,2,4-oxadiazole substituted analogue **21** (Scheme 1). The appropriate methyl 4-amino-6-chloronicotinate (**44**; R<sup>1</sup>=*N*-Boc-piperidin-4-ylmethyl) was hydrolysed to the acid **45**. The acid **45** was converted to the amide under standard conditions and the pyrazine introduced by Buchwald reaction as before, to give **13** after deprotection. Secondary amides **14** and **15** were prepared from the intermediate ester (**44**; R<sup>1</sup>=*N*-Boc-piperidin-4-ylmethyl) through conversion to **46** before hydrolysis and coupling of the crude acid to aniline or ethylamine. Deprotection gave **14** and **15**. Alternatively, the intermediate methyl ester **46** was converted to the acid by S<sub>N</sub>2 dealkylation with lithium iodide in pyridine. The crude acid was coupled with *N*'-hydroxyacetimidamide and cyclized at high temperature to yield the 1,2,4-oxadiazole **21**.

General procedures were developed for the synthesis of the *C*-5 alkenyl, aryl and heteroaryl substituted analogues **17**, **19**, **20**, **22-34** (Scheme 2). 2-Chloropyridin-4-amine (**47**) was iodinated to give 2-chloro-5-iodopyridin-4-amine (**48**).<sup>42</sup> Introduction of *C*-4 amine substituents was effected by alkylation of the sodium anion of **48** with either *tert*-butyl 4-(bromomethyl)piperidine-1-carboxylate or the appropriate enantiomerically pure *tert*-butyl 2-((tosyloxy)methyl)morpholine-4-carboxylates to give the substituted iodopyridines **49**. Suzuki couplings to the iodides **49** using vinyl, aryl and heteroaryl boronic acids or boronate esters generated the chloropyridines **50**. In turn, these were subject to Buchwald coupling with 5-

aminopyrazine-2-carbonitrile followed by *N*-Boc deprotection to give the test compounds. For the thiazole analogue **30**, the Suzuki coupling step was replaced with a Stille coupling using 5-methyl-2-(tributylstannyl)thiazole.

**Scheme 2.** Preparation of compounds **16-20** and **22-38**.<sup>a</sup>

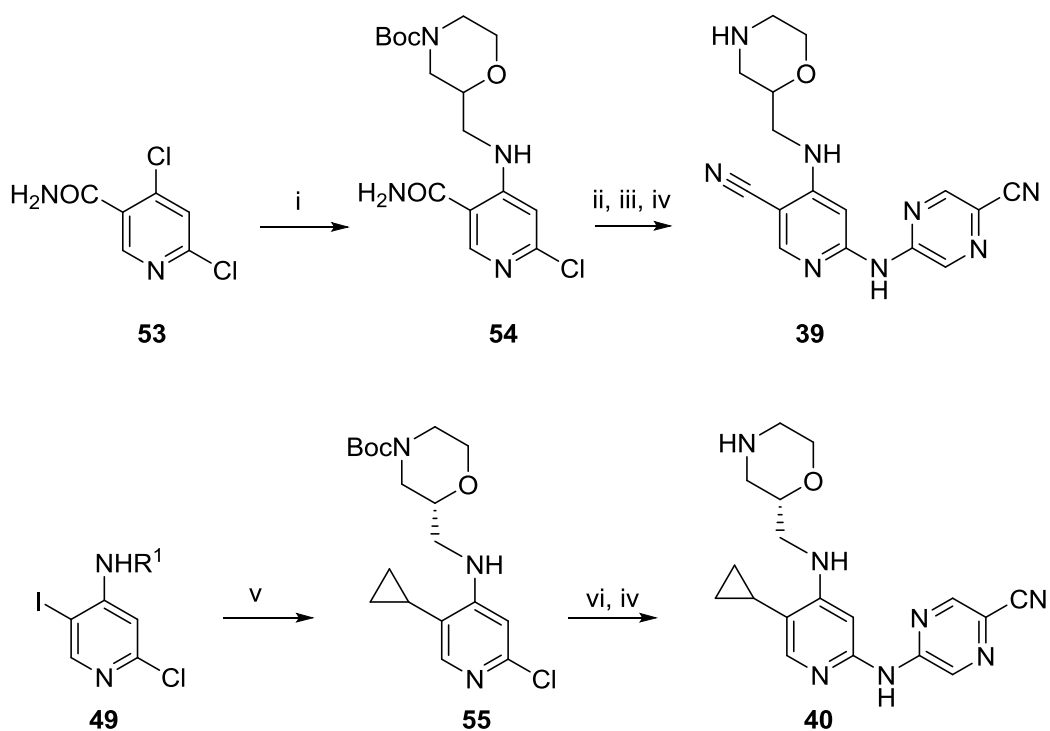


<sup>a</sup> Reagents and conditions: (i) ICl, KOAc, AcOH, 70 °C, 5 h; (ii) R<sup>1</sup>Br or R<sup>1</sup>OTs, NaH, DMF, 80 °C, 2 h; (iii) R<sup>2</sup>B(OR)<sub>2</sub>, (Ph<sub>3</sub>P)<sub>4</sub>Pd, Na<sub>2</sub>CO<sub>3</sub> (0.5M, H<sub>2</sub>O), MeCN, 100 °C (microwave irradiation), 20 min; (iv) 5-aminopyrazine-2-carbonitrile, Pd<sub>2</sub>(dba)<sub>3</sub>, xantphos, Cs<sub>2</sub>CO<sub>3</sub>, toluene, 150 °C (microwave irradiation), 1 h; (v) CF<sub>3</sub>CO<sub>2</sub>H, CH<sub>2</sub>Cl<sub>2</sub>, r.t.; (vi) 5-methyl-2-(tributylstannyl)thiazole, (Ph<sub>3</sub>P)<sub>4</sub>Pd, toluene, 90 °C, 18 h; (vii) HCl, dioxane, r.t., 1 h; (viii)

$R^3CCH$ , CuI, Pd(PH<sub>3</sub>P)<sub>2</sub>Cl<sub>2</sub>, Et<sub>3</sub>N, DMF, 120 °C (microwave irradiation), 10 min; (ix) H<sub>2</sub>, 10% Pd/C, EtOH, r.t., 18 h.

The above procedures were adapted for the synthesis of the *C*-5 alkynyl substituted analogues **18** and **35-38** (Scheme 2). The iodopyridines **49** were subject to Sonogashira couplings to give the alkynylpyridines **52**, followed by introduction of the pyrazine by Buchwald reaction and *N*-deprotection. Synthesis of the *C*-5 alkyl substituted analogue **16** was achieved starting from the appropriate protected 5-alkynyl-2-chloropyridine (**52**; R<sup>1</sup> = *N*-Boc-piperidin-4-yl-methyl, R<sup>3</sup> = <sup>t</sup>BuMe<sub>2</sub>SiOCH<sub>2</sub>), which was coupled to 5-aminopyrazine-2-carbonitrile using Buchwald conditions, followed by hydrogenation of the alkyne to the saturated alkyl chain (Scheme 2). The *N*-Boc and *O*-*tert*-butyl-dimethylsilyl protecting groups were removed using trifluoroacetic acid.

**Scheme 3.** Preparation of compounds **39** and **40**.<sup>a</sup>



<sup>a</sup> Reagents and conditions: (i) *tert*-Butyl (*rac*)-2-(aminomethyl)morpholine-4-carboxylate, Et<sub>3</sub>N, *t*-BuOH, 120 °C (microwave irradiation), 1.5 h; (ii) (CF<sub>3</sub>CO)<sub>2</sub>, Et<sub>3</sub>N, CH<sub>2</sub>Cl<sub>2</sub>, 0 °C, 30 min; (iii) 5-aminopyrazine-2-carbonitrile, Pd<sub>2</sub>(dba)<sub>3</sub>, BINAP, K<sub>3</sub>PO<sub>4</sub>, dioxane, 150 °C (microwave irradiation), 1 h; (iv) CF<sub>3</sub>CO<sub>2</sub>H, CH<sub>2</sub>Cl<sub>2</sub>, r.t.; (v) cyclopropylboronic acid pinacol ester, (Ph<sub>3</sub>P)<sub>4</sub>Pd, Na<sub>2</sub>CO<sub>3</sub> (0.5M, H<sub>2</sub>O), MeCN, 130 °C (microwave irradiation), 1.5 h; (vi) 5-aminopyrazine-2-carbonitrile, Pd<sub>2</sub>(dba)<sub>3</sub>, xantphos, Cs<sub>2</sub>CO<sub>3</sub>, dioxane, 130 °C (microwave irradiation), 45 min.

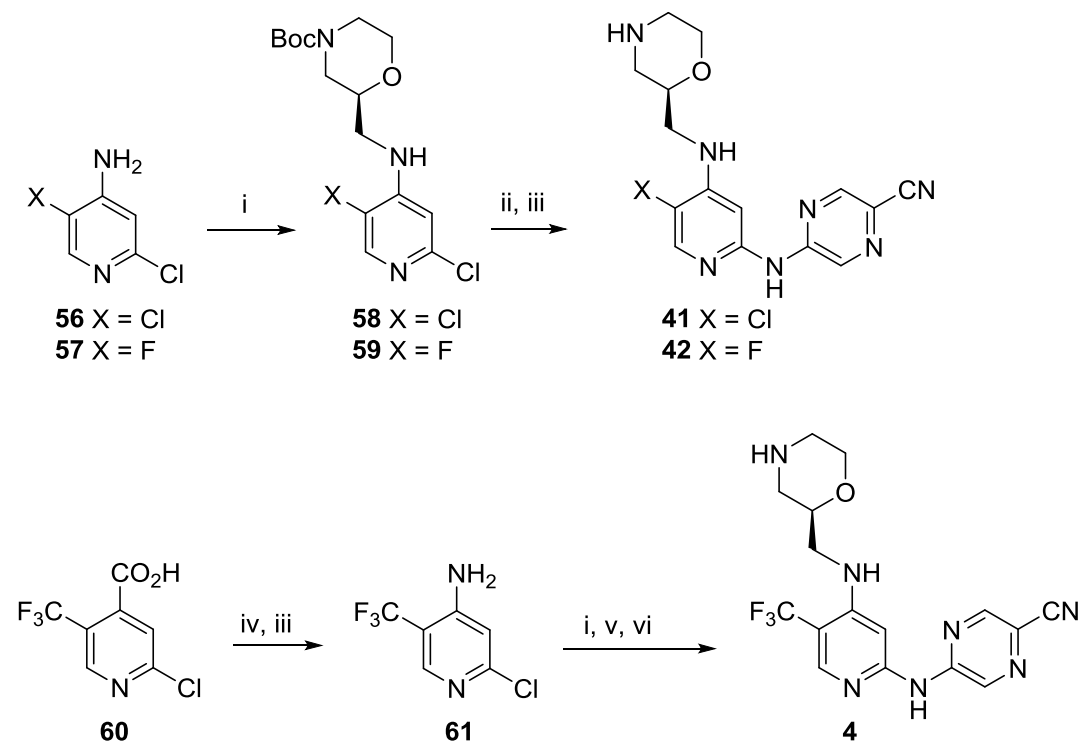
Synthesis of the *C*-5 nitrile analogue **39** was begun by selective S<sub>N</sub>Ar displacement of 4,6-dichloronicotinamide **53** using *tert*-butyl (*rac*)-2-(aminomethyl)morpholine-4-carboxylate to yield the chloropyridine **54** (Scheme 3). The nitrile was then introduced by dehydration of the primary amide using trifluoroacetic anhydride. Buchwald coupling to install the pyrazine and *N*-deprotection followed as before.

Synthesis of the *C*-5 cyclopropyl analogue **40** was achieved by reacting the appropriate 5-iodopyridine (**49**; R<sup>1</sup> = (*R*)-*N*-Boc-morpholin-2-yl-methyl) with cyclopropylboronic acid pinacol ester under Suzuki coupling conditions to give **55**, followed by Buchwald coupling of the pyrazine and *N*-deprotection (Scheme 3).

General procedures were developed for the synthesis of the *C*-5 chloro- and fluoro-substituted Analogues **41** and **42** (Scheme 4). Commercially available pyridines **56** and **57** were *N*-alkylated with *tert*-butyl (*R*)-2-((tosyloxy)methyl)morpholine-4-carboxylate to give the chloropyridines **58** and **59**, respectively, which were subject to Buchwald coupling and *N*-deprotection to generate **41** and **42**.

Synthesis of the *C*-5 trifluoromethyl substituted analogue **4** was begun by conversion of the commercially available 2-chloro-5-(trifluoromethyl)isonicotinic acid (**60**) to the 4-aminopyridine **61** by a Curtius-Hoffman reaction sequence<sup>43</sup> (Scheme 4). *N*-Alkylation using *tert*-butyl (*R*)-2-((tosyloxy)methyl)morpholine-4-carboxylate, followed by Buchwald coupling of 5-aminopyrazine-2-carbonitrile and morpholine *N*-deprotection completed the synthesis of **4**.

**Scheme 4.** Preparation of compounds **4**, **41** and **42**.<sup>a</sup>



<sup>a</sup> Reagents and conditions: (i) *tert*-Butyl (*R*)-2-((tosyloxy)methyl)morpholine-4-carboxylate, NaH, DMF, 80 °C, 2.5 h; (ii) 5-aminopyrazine-2-carbonitrile, Pd<sub>2</sub>(dba)<sub>3</sub>, xantphos, Cs<sub>2</sub>CO<sub>3</sub>, dioxane, 150 °C (microwave irradiation), 60 min; (iii) CF<sub>3</sub>CO<sub>2</sub>H, CH<sub>2</sub>Cl<sub>2</sub>, r.t.; (iv) diphenyl phosphorazidate, Et<sub>3</sub>N, <sup>t</sup>BuOH, toluene, 105 °C, 5 h; (v) 5-aminopyrazine-2-carbonitrile, Pd<sub>2</sub>(dba)<sub>3</sub>, BINAP, Cs<sub>2</sub>CO<sub>3</sub>, dioxane, 150 °C (microwave irradiation), 1 h; (vi) CF<sub>3</sub>CO<sub>2</sub>H, <sup>t</sup>Pr<sub>3</sub>SiH, CH<sub>2</sub>Cl<sub>2</sub>, r.t., 1 h.

## CONCLUSION

Multi-parameter lead optimization of a series of 5-((4-aminopyridin-2-yl)amino)pyrazine-2-carbonitriles was conducted to identify potent and selective CHK1 inhibitors that potentiated the efficacy of genotoxic agents *in vitro* and *in vivo*. The use of cellular mechanism of action assays to give an integrated assessment of compound selectivity was critical to drive the *in vitro* optimization of the series and resulted in a highly CHK1 selective, ATP-competitive inhibitor. In particular, selective effects in cells were dependent on the size of a substituent directed away

from the CHK1 kinase active site. Lipophilicity and basicity were observed to drive both CHK1 potency and off-target hERG ion channel activity with some overlapping structure-activity relationships. An acceptable therapeutic window over hERG inhibition was achieved by identifying molecules which gave potent CHK1 affinity and cellular activity through minimizing the size of the C-5 substituent.

Augmenting *in vitro* assays with an efficient *in vivo* PK screening strategy was important to select compounds with favorable oral PK properties from this series. In tandem, *in vivo* PD studies identified compounds giving prolonged target engagement following single oral dose, which is anticipated as important for the clinical success of CHK1 inhibition in combination with genotoxic drugs. Compounds with the desired PK-PD profile demonstrated efficacy *in vivo* in this setting. Compound **4** was profiled in depth and showed a favorable physicochemical, PK and PD-efficacy profile. The high affinity and low predicted human clearance of the compound supported predictions of low doses to humans. This mitigated the residual *in vitro* hERG activity, confirmed by an *in vivo* cardiovascular pharmacology study (data not shown). Compound **4** (CCT245737) was selected for progression to preclinical development.

## EXPERIMENTAL SECTION

**Chemistry: General Information.** Reactions were carried out under N<sub>2</sub>. Organic solutions were dried over magnesium sulfate or sodium sulfate. Starting materials and solvents were purchased from commercial suppliers and were used without further purification. Reactions heated by microwave irradiation were carried out using a Biotage Initiator microwave reactor. Flash silica column chromatography was performed using Merck silica gel 60 (0.025-0.04 mm). Gradient silica column chromatography was performed with a Biotage SP1 medium pressure

chromatography system, using prepacked silica gel cartridges. Ion exchange chromatography was performed using Isolute Flash SCX-II (acidic) or Flash NH2 (basic) resin cartridges. <sup>1</sup>H NMR spectra were recorded on a Bruker AMX500 instrument at 500 MHz or on a Bruker Avance instrument at 400MHz using internal deuterium locks. Chemical shifts (δ) are reported relative to TMS (δ=0) and/or referenced to the solvent in which they were measured. Compounds were assessed for purity by tandem HPLC-MS. Combined HPLC-MS analyses were recorded using a Waters Alliance 2795 separations module and Waters/Micromass LCT mass detector with HPLC performed using Supelco DISCOVERY C18, 50 mm x 4.6 mm or 30 mm x 4.6 mm i.d. columns, or using an Agilent 6210 TOF HPLC-MS with a Phenomenex Gemini 3 μm C18 (3 cm x 4.6 mm i.d.) column. Both HPLC systems were run at a temperature of 22 °C with gradient elution of 10-90% MeOH/0.1% aqueous formic acid at a flow rate of 1 mL/min and a run time of 3.5, 4 or 6 min. UV detection was at 254 nm and ionisation was by positive or negative ion electrospray. The molecular weight scan range was 50-1000 amu. Biologically evaluated compounds gave >95% purity as determined by these methods.

**Synthesis of compound 4.** *(R)*-5-(4-(Morpholin-2-ylmethylamino)-5-(trifluoromethyl)pyridin-2-ylamino)pyrazine-2-carbonitrile (**4**). NaH (60% in oil, 33 mg, 0.81 mmol) was added to a solution of 2-chloro-5-(trifluoromethyl)pyridin-4-amine (**61**) (80 mg, 0.41 mmol) in DMF (4 mL) and the mixture was stirred at rt for 10 min. The temperature was raised to 80 °C and *(R)*-*tert*-butyl 2-(tosyloxymethyl)morpholine-4-carboxylate (181 mg, 0.488 mmol) was added portion wise. The reaction mixture was stirred at 80 °C for 2 h, then cooled to rt. The mixture was partitioned between saturated aqueous NaHCO<sub>3</sub> and EtOAc. The combined organic layers were washed with brine, dried, filtered and concentrated. Flash column chromatography, eluting with a gradient of 10–20% EtOAc–hexanes, gave *(S)*-*tert*-butyl 2-((2-chloro-5-

(trifluoromethyl)pyridin-4-ylamino)methyl)morpholine-4-carboxylate (118 mg, 0.30 mmol, 73%).  $^1\text{H}$  NMR ( $\text{CDCl}_3$ , 500 MHz)  $\delta$  8.24 (s, 1H), 6.61 (s, 1H), 5.32 (br s, 1H), 3.96 – 3.94 (m, 3H), 3.70 – 3.65 (m, 1H), 3.58 (ddd,  $J = 11.5$ , 11.5 and 2.6 Hz, 1H), 3.37 – 3.32 (m, 1H), 3.21 – 3.18 (m, 1H), 2.99 (br s, 1H), 2.77 (br s, 1H), 1.49 (s, 9H);  $^{13}\text{C}$  NMR ( $\text{CD}_3\text{OD}$ , 125 MHz)  $\delta$  155.4, 154.3, 152.6, 147.4 (q,  $J_{\text{CF}} = 6.1$  Hz), 124.7 (q,  $J_{\text{CF}} = 269.8$  Hz), 108.6 (q,  $J_{\text{CF}} = 30.2$  Hz), 106.0, 79.6, 73.8, 66.2, 46.2 (br), 44.5, 45.0 (br), 28.4 (3C); LCMS (3.5 min)  $t_{\text{R}} = 2.62$  min;  $m/z$  ( $\text{ESI}^+$ ) 396 ( $\text{M}+\text{H}^+$ ); HRMS  $m/z$  calcd for  $\text{C}_{16}\text{H}_{22}\text{ClF}_3\text{N}_3\text{O}_3$  ( $\text{M} + \text{H}$ ) 396.1296, found 396.1292.

Dioxane (2.53 mL) was added to a mixture of (*S*)-*tert*-butyl 2-((2-chloro-5-(trifluoromethyl)pyridin-4-ylamino)methyl)morpholine-4-carboxylate (100 mg, 0.25 mmol), 5-aminopyrazine-2-carbonitrile (42.5 mg, 0.35 mmol),  $\text{Pd}_2\text{dba}_3$  (19 mg, 0.02 mmol),  $\text{Cs}_2\text{CO}_3$  (165 mg, 0.50 mmol) and BINAP (25 mg, 0.04 mmol). Argon was bubbled through the suspension for 5 min. The mixture was heated by microwave irradiation at 150 °C for 1 h. The reaction mixture was cooled to rt and purified by ion exchange chromatography on SCX-II acidic resin, eluting with MeOH then 2M  $\text{NH}_3$  in MeOH. The basic fractions were combined and concentrated. Preparative thin layer chromatography, eluting with 2% MeOH– $\text{CH}_2\text{Cl}_2$ , gave (*S*)-*tert*-butyl 2-((2-(5-cyanopyrazin-2-ylamino)-5-(trifluoromethyl)pyridin-4-ylamino)methyl)morpholine-4-carboxylate (69 mg, 0.144 mmol, 57%).  $^1\text{H}$  NMR ( $\text{CD}_3\text{OD}$ , 500 MHz)  $\delta$  8.97 (br s, 1H), 8.66 (br s, 1H), 8.19 (s, 1H), 7.34 (br s, 1H), 4.04 (br d,  $J = 12.9$  Hz, 1H), 3.94 (br d,  $J = 10.5$  Hz, 1H), 3.86 (ddd,  $J = 13.4$ , 1.3 and 1.3 Hz, 1H), 3.72 – 3.71 (m, 1H), 3.54 (ddd,  $J = 11.7$ , 11.7 and 2.5 Hz, 1H), 3.46 – 3.39 (m, 2H), 3.00 (br s, 1H), 2.77 (br s, 1H), 1.47 (s, 9H);  $^{13}\text{C}$  NMR ( $(\text{CD}_3)_2\text{SO}$ , 125 MHz)  $\delta$  156.2, 154.3, 152.3, 152.0, 147.6, 146.4 (q,  $J_{\text{CF}} = 5.2$  Hz), 137.3, 125.2 (q,  $J_{\text{CF}} = 271.8$  Hz), 119.2, 117.5, 104.9 (q,  $J_{\text{CF}} = 21.0$  Hz), 93.9, 79.6, 73.0, 66.3, 46.7 (br), 44.9 (br), 43.7 (br), 28.4 (3C); LCMS (3.5 min)  $t_{\text{R}} = 2.51$  min;  $m/z$  ( $\text{ESI}^+$ ) 480 ( $\text{M}+\text{H}^+$ ); HRMS calcd for

$C_{21}H_{25}F_3N_7O_3$  (M + H) 480.1966, found 480.1971. The above procedures were repeated to produce additional starting material for the next stage:  $CF_3CO_2H$  (4.7 mL, 61 mmol) was added to a solution of (*S*)-*tert*-butyl 2-((2-(5-cyanopyrazin-2-ylamino)-5-(trifluoromethyl)pyridin-4-ylamino)methyl)-morpholine-4-carboxylate (206 mg, 0.4 mmol) and  $(^iPr)_3SiH$  (0.56 mL, 2.8 mmol) in  $CH_2Cl_2$  (50 mL). The solution was stirred at rt for 1 h then solvents were removed by evaporation. The residue was purified by ion exchange chromatography on SCX-II acidic resin, eluting with MeOH then 2M  $NH_3$  in MeOH. The basic fractions were combined and concentrated. Trituration with 10% MeOH- $CH_2Cl_2$  gave **4** (116 mg) as an amorphous solid. Purification of the mother liquids by preparative thin layer chromatography, eluting with 5% MeOH- $CH_2Cl_2$ , gave additional material (22 mg) of similar purity. The two batches of material obtained were combined, re-dissolved in MeOH, and solvent was removed by evaporation to give **4** (138 mg, 0.364 mmol, 85%) as a pale yellow amorphous solid.  $^1H$  NMR ( $(CD_3)_2SO$ , 500 MHz)  $\delta$  10.7 (br s, 1H), 9.10 (d,  $J = 1.4$  Hz, 1H), 8.77 (d,  $J = 1.4$  Hz, 1H), 8.20 (s, 1H), 7.19 (s, 1H), 6.32 (br t,  $J = 5.5$  Hz, 1H), 3.75 (br d,  $J = 11.0$  Hz, 1H), 3.64 – 3.59 (m, 1H), 3.43 (ddd,  $J = 10.7, 10.7$  and  $3.4$  Hz, 1H), 3.22 (m, 2H), 2.82 (dd,  $J = 12.1$  and  $2.1$  Hz, 1H), 2.67 – 2.59 (m, 2H), 2.42 (dd,  $J = 12.1$  and  $10.0$  Hz, 1H);  $^{13}C$  NMR ( $(CD_3)_2SO$ , 125 MHz)  $\delta$  155.7, 151.9, 151.6, 147.2, 145.9 (q,  $J_{CF} = 6.3$  Hz), 136.8, 124.8 (q,  $J_{CF} = 270.9$  Hz), 118.9, 117.1, 104.4 (q,  $J_{CF} = 30.0$  Hz), 93.2, 73.6, 67.2, 48.9, 45.4, 44.9; LCMS (3.5 min)  $t_R = 1.17$  min;  $m/z$  (ESI $^+$ ) 380 (M+H $^+$ ); HRMS  $m/z$  calcd for  $C_{16}H_{17}F_3N_7O$  (M + H) 380.1441, found 380.1438.

*2-Chloro-5-(trifluoromethyl)pyridin-4-amine* (**61**).  $Et_3N$  (2.80 mL, 20 mmol) was added to a solution of 2-chloro-5-(trifluoromethyl)isonicotinic acid (**60**; 1.5 g, 6.6 mmol) and diphenyl phosphorazidate (2.14 mL, 9.9 mmol) in  $^iBuOH$  (12 mL) and toluene (13.5 mL). The solution was stirred at 105°C for 5 h. The reaction mixture was cooled to rt and solvents were evaporated.

The residue was partitioned between water and EtOAc. The combined organic layers were washed with brine, dried, filtered and concentrated. Flash column chromatography, eluting with 10% EtOAc–hexanes, gave *tert*-butyl (2-chloro-5-(trifluoromethyl)pyridin-4-yl)carbamate (1.24 g, 4.2 mmol, 63%). <sup>1</sup>H NMR (CDCl<sub>3</sub>, 500MHz) δ 8.50 (s, 1H), 8.45 (s, 1H), 7.00 (br s, 1H), 1.57 (s, 9H); <sup>13</sup>C NMR (CDCl<sub>3</sub>, 125 MHz) δ 156.3, 150.4, 146.8 (q, *J*<sub>CF</sub> = 7.1 Hz), 144.9, 123.0 (q, *J*<sub>CF</sub> = 275.8 Hz), 112.7, 111.5 (q, *J*<sub>CF</sub> = 31.2 Hz), 82.9, 27.6 (3C); LCMS (3.5 min) *t*<sub>R</sub> = 2.77 min; *m/z* (ESI<sup>+</sup>) 297 (M+H<sup>+</sup>); HRMS calcd for C<sub>11</sub>H<sub>13</sub>ClF<sub>3</sub>N<sub>2</sub>O<sub>2</sub> (M + H) 297.0612, found 297.0627.

CF<sub>3</sub>CO<sub>2</sub>H (6.44 mL, 84 mmol) was added to a solution of *tert*-butyl (2-chloro-5-(trifluoromethyl)pyridin-4-yl)carbamate (1.24 g, 4.2 mmol) in CH<sub>2</sub>Cl<sub>2</sub> (16.5 mL). The solution was stirred at rt for 5 h. Solvents were removed by evaporation and the residue was purified by ion exchange chromatography on SCX-II acidic resin, eluting with MeOH then 2M NH<sub>3</sub> in MeOH. The basic fractions were combined to give 2-chloro-5-(trifluoromethyl)pyridin-4-amine (**61**; 0.736 g, 3.8 mmol, 90%). <sup>1</sup>H NMR (CDCl<sub>3</sub>, 500MHz) δ 8.30 (s, 1H), 6.66 (s, 1H), 4.77 (br s, 2H); <sup>13</sup>C NMR (CD<sub>3</sub>OD, 125 MHz) δ 154.0, 146.8 (q, *J*<sub>CF</sub> = 6.2 Hz), 124.2 (q, *J*<sub>CF</sub> = 268.0 Hz), 108.9, 108.7 (q, *J*<sub>CF</sub> = 30.8 Hz), (one quaternary carbon not observed); LCMS (3.5 min) *t*<sub>R</sub> = 1.82 min; *m/z* (ESI<sup>+</sup>) 197 (M+H<sup>+</sup>); HRMS *m/z* calcd for C<sub>6</sub>H<sub>5</sub>ClF<sub>3</sub>N<sub>2</sub> (M + H) 197.0088, found 197.0082.

**Biochemical assays.** *In vitro* assays for inhibition of CHK1 and CHK2 were carried out as described previously.<sup>18,19</sup>

**Cellular assays.** Assays for the determination of checkpoint abrogation, antiproliferative activity, and potentiation of genotoxic drug efficacy in cancer cell lines were carried out as described previously.<sup>19,21</sup>

**Crystallography.** Crystallography of CHK1 kinase domain was carried out as described previously.<sup>20</sup> Data were integrated with XDS<sup>44</sup>, imported with POINTLESS<sup>S2</sup>, then scaled and merged with AIMLESS<sup>45</sup>. Following molecular replacement as previously described, the structure was refined with COOT<sup>46</sup> and BUSTER<sup>47</sup>. TLS parameters were generated with PHENIX<sup>48</sup>. Ligand geometry restraints were generated with GRADE<sup>49</sup>/MOGUL<sup>50</sup>.

**In vivo assays.** All experiments using animals were performed in accordance with the local Animal Welfare and Ethical Review Board, the UK Home Office Animals Scientific Procedures Act 1986 and with the United Kingdom National Cancer Research Institute guidelines for the welfare of animals in cancer research.<sup>51</sup> The ICR does not undertake research in non-rodent species and requires internal ethical review when such studies are sponsored by organizations with whom we collaborate. Collaborator-sponsored non-rodent pharmacology studies of compound **4** necessary for the prediction of therapeutic window were approved by the ICR Animal Welfare and Ethics Review Board and were conducted in full compliance with national regulations at AAALAC accredited R&D sites. Detailed experimental procedures are reported in the Supporting Information.

## ASSOCIATED CONTENT

**Supporting Information.** Mouse liver microsome stability of selected compounds; Kinase inhibition profile of **4**; Potentiation of genotoxic efficacy in cancer cell lines by **4**; Cardiac ion channel inhibition profile of **4**; Experimental methods for the synthesis of compounds **3** and **5-42**; Experimental methods for *in silico* classification model; Experimental methods for *in vivo* procedures; Experimental methods for MRI; Data collection and refinement statistics for the

crystal structure of CHK1 with **12**; HPLC data for key compounds; <sup>1</sup>H and <sup>13</sup>C NMR spectra for compounds **3-42**.

This material is available free of charge via the Internet at <http://pubs.acs.org>.

**PDB ID Codes:** 5F4N

## AUTHOR INFORMATION

### Corresponding Author

\* E-mail: [ian.collins@icr.ac.uk](mailto:ian.collins@icr.ac.uk). Tel: +44 2087224000.

### Author Contributions

The manuscript was written through contributions of all authors. All authors have given approval to the final version of the manuscript.

### Funding Sources

This work was supported by Cancer Research UK [CUK] grant numbers C309/A8274 and C309/A11566, the Cancer Research UK and EPSRC Cancer Imaging Centre, in association with the MRC and Department of Health (England) grant number C1060/A10334, the Institute of Cancer Research, and Sareum Ltd.

## ACKNOWLEDGMENTS

The authors thank Dr Amin Mirza, Dr Maggie Liu and Mr Meirion Richards for assistance in analytical chemistry and spectroscopy, Professor Owen Samson for the provision of KPC1 GEMM pancreatic tumor cells, and Professor Louis Chesler for provision of TH-MYCN mice. We acknowledge Simcyp Ltd for license to use the Simcyp population-based ADME Simulator.

## ABBREVIATIONS USED

AMPK, 5'-AMP-activated protein kinase ATM; ataxia telangiectasia mutated; ATR, ataxia telangiectasia and Rad3-related; BINAP, 2,2'-bis(diphenylphosphino)-1,1'-binaphthyl); CDC25, cell division cycle 25; CHK1, checkpoint kinase 1; CHK2, checkpoint kinase 2; CDK1, cyclin dependent kinase 1; CLint, intrinsic clearance; DDR, DNA damage response; DELFIA, Dissociation-Enhanced Lanthanide Fluorescent Immunoassay; DNA, deoxyribonucleic acid; G1, Gap1 phase; G2, Gap 2 phase; GEMM, genetically engineered mouse model; HBD, hydrogen bond donors; hERG, human ether-a-go-go-related gene; KRAS, V-Ki-ras2 Kirsten rat sarcoma viral oncogene homolog; MLM, mouse liver microsomes; MRI, magnetic resonance imaging; MTD, maximum tolerated dose; MYC, v-myc avian myelocytomatosis viral oncogene homolog; MYCN, v-myc avian myelocytomatosis viral oncogene neuroblastoma derived homolog; *N*-Boc, *N*-tert-butyloxycarbonyl; NSCLC, non-small cell lung cancer; PBPK, physiological-based pharmacokinetic; PD, pharmacodynamic; PK, pharmacokinetic; RNA, ribonucleic acid; S, Synthesis phase; SRB, sulforhodamine B.

## REFERENCES

1. Dai, Y.; Grant, S. New insights into checkpoint kinase 1 in the DNA damage response signalling network. *Clin. Cancer Res.* **2010**, *16*, 376-383.
2. Smith, J.; Tho, L. M.; Xu, N.; Gillespie, D. A. The ATM-Chk2 and ATR-Chk1 pathways in DNA damage signaling and cancer. *Adv. Cancer Res.* **2010**, *108*, 73-112.
3. Clarke, C.A.; Clarke, P. R. DNA-dependent phosphorylation of CHK1 and claspin in human cell-free system. *Biochem. J.* **2005**, *388*, 705-712.

4. Xiao, Z.; Chen, Z.; Gunasekera, A. H.; Sowin, T. J.; Rosenberg, S. H.; Fesik, S.; Zhang, H. Chk1 mediates S and G2 arrests through Cdc25A degradation in response to DNA-damaging agents. *J. Biol. Chem.* **2003**, *278*, 21767-21773.
5. Sorensen, C. S.; Hansen, L. T.; Dziegielewska, J.; Syljuasen, R. G.; Lundin, C.; Bartek, J.; Helleday, T. The cell-cycle checkpoint kinase chk1 is required for mammalian homologous recombination repair. *Nat. Cell Biol.* **2005**, *7*, 195-201.
6. Chen, T.; Stephens, P. A.; Middleton, F. K.; Curtin, N. J. Targeting the S and G2 checkpoint to treat cancer. *Drug Discov. Today* **2012**, *17*, 194-202.
7. Garrett, M. D.; Collins, I. Anticancer therapy with checkpoint inhibitors: what, when and where? *Trends Pharmacol. Sci.* **2011**, *32*, 308-316.
8. Ma, C. X.; Janetka, J. W.; Piwnicka-Worms, H. Death by releasing the breaks: Chk1 inhibitors as cancer therapeutics. *Trends Mol. Med.* **2011**, *17*, 88-96.
9. Cole, K. A.; Huggins, J.; Laquaglia, M.; Hulderman, C. E.; Russell, M. R.; Bosse, K.; Diskin, S. J.; Attiyeh, E. F.; Sennett, R.; Norris, G.; Laudenslager, M.; Wood, A. C.; Mayes, P. A.; Jagannathan, J.; Winter, C.; Mosse, Y. P.; Maris, J. M. RNAi screen of the protein kinome identifies checkpoint kinase 1 (CHK1) as a therapeutic target in neuroblastoma. *Proc. Natl. Acad. Sci. U.S.A.* **2011**, *108*, 3336-3341.
10. Höglund, A.; Nilsson, L. M.; Muralidharan, S. V.; Hasvold, L. A.; Merta, P.; Rudelius, M.; Nikolova, V.; Keller, U.; Nilsson, J. A. Therapeutic implications for the induced levels of Chk1 in Myc expressing cancer cells. *Clin. Cancer Res.* **2011**, *17*, 7067-7079.

11. Brooks, K.; Oakes, V.; Edwards, B.; Ranall, M.; Leo, P.; Pavey, S.; Pinder, A.; Beamish, H.; Mukhopadhyay, P.; Lambie, D.; Gabrielli, B. A potent Chk1 inhibitor is selectively cytotoxic in melanomas with high levels of replicative stress. *Oncogene* **2013**, *32*, 788-796.
12. Albiges, L.; Goubar, A.; Scott, V.; Vicier, C.; Lefèbvre, C.; Alsafadi, S.; Commo, F.; Saghatchian, M.; Lazar, V.; Dessen, P.; Delalogue, S.; André, F.; Quidville, V. Chk1 as a new therapeutic target in triple-negative breast cancer. *Breast* **2014**, *23*, 250-258.
13. McNeely, S.; Beckmann, R.; Bence Lin, A. K. CHEK again: revisiting the development of CHK1 inhibitors for cancer therapy. *Pharmacol. Ther.* **2014**, *142*, 1-10.
14. Walton, M. I.; Eve, P. D.; Hayes, A.; Valenti, M. R.; De Haven Brandon, A. K.; Box, G.; Hallsworth, A.; Smith, E. L.; Boxall, K. J.; Lainchbury, M.; Matthews, T. P.; Jamin, Y.; Robinson, S. P.; Aherne, G. W.; Reader, J. C.; Chesler, L.; Raynaud, F. I.; Eccles, S. A.; Collins, I.; Garrett, M. D. CCT244747 is a novel, potent and selective CHK1 inhibitor with oral efficacy alone and in combination with genotoxic anticancer drugs. *Clin. Cancer Res.* **2012**, *18*, 5650-5661.
15. Blackwood, E.; Epler, J.; Yen, I.; Flagella, M.; O'Brien, T.; Evangelista, M.; Schmidt, S.; Xiao, Y.; Choi, J.; Kowanetz, K.; Ramiscal, J.; Wong, K.; Jakubiak, D.; Yee, S.; Cain, G.; Gazzard, L.; Williams, K.; Halladay, J.; Jackson, P. K.; Malek, S. Combination drug scheduling defines a "window of opportunity" for chemopotential of gemcitabine by an orally bioavailable, selective ChK1 inhibitor, GNE-900. *Mol. Cancer Ther.* **2013**, *12*, 1968-1980
16. Infante, J. R.; Hollebecque, A.; Postel-Vinay, S.; Bauer, T.; Blackwood, B.; Evangelista, M.; Mahrus, S.; Peale, F.; Lu, X.; Sahasranaman, S.; Zhu, R.; Chen, Y.; Ding, X.; Murray,

- E.; Schutzman, J.; Lauchle, J.; Soria, J.; LoRusso, P. Phase I study of GDC-0425, a checkpoint kinase 1 inhibitor, in combination with gemcitabine in patients with refractory solid tumors. In: Proceedings of the 106th Annual Meeting of the American Association for Cancer Research; 2015 Apr 18-22; Philadelphia, PA. Philadelphia (PA): AACR; 2015. Abstract nr CT139.
17. Stumpf, A.; Cheng, Z. K.; Wong, B.; Reynolds, M.; Angelaud, R.; Girotti, J.; Deese, A.; Gu, C.; Gazzard, L. Development of an expedient process for the multi-kilogram synthesis of Chk1 inhibitor GDC-0425. *Org. Process Res. Dev.* **2015**, *19*, 661-672.
18. Lainchbury, M.; Matthews, T. P.; McHardy, T.; Boxall, K. J.; Walton, M. I.; Eve, P. D.; Hayes, A.; Valenti, M. R.; de Haven Brandon A. K.; Box, G.; Aherne, G. W.; Reader, J. C.; Raynaud, F. I.; Eccles, S. A.; Garrett, M. D.; Collins, I. Discovery of 3-alkoxyamino-5-(pyridin-2-ylamino)pyrazine-2-carbonitriles as selective, orally bioavailable CHK1 inhibitors. *J. Med. Chem.* **2012**, *55*, 10229-10240.
19. Reader, J. C.; Matthews, T. P.; Klair, S.; Cheung, K. J.; Scanlon, J.; Proisy, N.; Addison, G.; Ellard, J.; Piton, N.; Taylor, S.; Cherry, M.; Fisher, M.; Boxall, K.; Burns, S.; Walton, M. I.; Westwood, I. M.; Hayes, A.; Eve, P.; Valenti, M.; de Haven Brandon, A.; Box, G.; van Montfort, R. L.; Williams, D. H.; Aherne, G. W.; Raynaud, F. I.; Eccles, S. A.; Garrett, M. D.; Collins, I. Structure-guided evolution of potent and selective CHK1 inhibitors through scaffold morphing. *J. Med. Chem.* **2011**, *54*, 8328-8342.
20. Walton, M. I.; Eve, P. D.; Hayes, A.; Valenti, M.; De Haven-Brandon, A.; Box, G.; Boxall, K. J.; Aherne, G. W.; Eccles, S. A.; Raynaud, F. I.; Williams, D. H.; Reader, J. C.; Collins,

- I.; Garrett, M. D. The preclinical pharmacology and therapeutic activity of the novel CHK1 inhibitor SAR-020106. *Mol. Cancer Ther.* **2010**, *9*, 89-100.
21. Walton, M. I.; Eve, P. D.; Hayes, A.; Henley, A. T. M. R.; De Haven Brandon, A. K.; Box, G.; Boxall, K. J.; Tall, M.; Swales, K.; Matthews, T. P.; McHardy, T.; Lainchbury, M.; Osborne, J.; Hunter, J. E.; Perkins, N. D.; Aherne, G. W.; Reader, J. C.; Raynaud, F. I.; Eccles, S. A.; Collins, I.; Garrett, M. D. The clinical development candidate CCT245737 is an orally active CHK1 inhibitor with preclinical activity in RAS mutant NSCLC and Eμ-MYC driven B-cell lymphoma. *Oncotarget* **2015**, *7*, 2329-2342.
22. Guzi, T. J.; Paruch, K.; Dwyer, M. P.; Labroli, M.; Shanahan, F.; Davis, N.; Taricani, L.; Wiswell, D.; Seghezzi, W.; Penafior, E.; Bhagwat, B.; Wang, W.; Gu, D.; Hsieh, Y.; Lee, S.; Liu, M.; Parry, D. Targeting the replication checkpoint using SCH 900776, a potent and functionally selective CHK1 inhibitor identified via high content screening. *Mol Cancer Ther.* **2011**, *10*, 591-602.
23. Anderson, V. E.; Walton, M. I.; Eve, P. D.; Boxall, K. J.; Antoni, L.; Caldwell, J. J.; Aherne, W.; Pearl, L. H.; Oliver, A. W.; Collins, I.; Garrett, M. D. CCT241533 is a potent and selective inhibitor of CHK2 that potentiates the cytotoxicity of PARP inhibitors. *Cancer Res.* **2011**, *71*, 463-472.
24. Carlessi, L.; Buscemi, G.; Larson, G.; Hong, Z.; Wu, J. Z.; Delia, D. Biochemical and cellular characterization of VRX0466617, a novel and selective inhibitor for the checkpoint kinase Chk2. *Mol. Cancer Ther.* **2007**, *6*, 935-944.

25. Xiao, Y.; Ramiscal, J.; Kowanetz, K.; Del Nagro, C.; Malek, S.; Evangelista, M.; Blackwood, E.; Jackson, P. K.; O'Brien, T. Identification of preferred chemotherapeutics for combining with a CHK1 inhibitor. *Mol. Cancer Ther.* **2013**, *12*, 2285-2295.
26. Jamieson, C.; Moir, E. M.; Rankovic, Z.; Wishart, G. Medicinal chemistry of hERG optimizations: highlights and hang-ups. *J. Med. Chem.* **2006**, *49*, 5029-5046.
27. Matthews, T. P.; Jones, A. M.; Collins, I. Structure-based design, discovery and development of checkpoint kinase inhibitors as potential anticancer therapies. *Expert Opin. Drug Discov.* **2013**, *6*, 621-640.
28. Tao, Z. F.; Wang, L.; Stewart, K. D.; Chen, Z.; Gu, W.; Bui, M. H.; Merta, P.; Zhang, H.; Kovar, P.; Johnson, E.; Park, C.; Judge, R.; Rosenberg, S.; Sowin, T.; Lin, N. H. Structure-based design, synthesis, and biological evaluation of potent and selective macrocyclic checkpoint kinase 1 inhibitors. *J. Med. Chem.* **2007**, *50*, 1514-1527.
29. Jamei, M.; Marciniak, S.; Feng, K.; Barnett, A.; Tucker, G.; Rostami-Hodjegan, A. The Simcyp population-based ADME simulator. *Expert Opin. Drug Metab. Toxicol.* **2009**, *5*, 211-223.
30. Determined at Cyprotex; <http://www.cyprotex.com>.
31. Sinha, S.; Ahire, D.; Wagh, S.; Mullick, D.; Sistla, R.; Selvakumar, K.; Cortes, J. C.; Putlur, S. P.; Mandlekar, S.; Johnson, B. M. Electrophilicity of pyridazine-3-carbonitrile, pyrimidine-2-carbonitrile, and pyridine-carbonitrile derivatives: a chemical model to describe the formation of thiazoline derivatives in human liver microsomes. *Chem. Res. Toxicol.* **2014**, *27*, 2052-2061.

32. Determined at The MRC Protein Phosphorylation and Ubiquitylation Unit, University of Dundee, U.K.; <http://www.ppu.mrc.ac.uk>.
33. Kerkela, R.; Woulfe, K. C.; Durand, J. B.; Vagnozzi, R.; Kramer, D.; Chu, T. F.; Beahm, C.; Chen, M. H.; Force, T. Sunitinib-induced cardiotoxicity is mediated by off-target inhibition of AMP-activated protein kinase. *Clin. Transl. Sci.* **2009**, *2*, 15-25.
34. Smyth, L. A.; Collins, I. Measuring and interpreting the selectivity of protein kinase inhibitors. *J. Chem. Biol.* **2009**, *2*, 131-151.
35. Schneider, G.; Schmid, R. M. Genetic alterations in pancreatic carcinoma. *Mol. Cancer.* **2003**, *2*, 15.
36. Mogi, A.; Kuwano, H. TP53 mutations in non-small cell lung cancer. *J. Biomed. Biotechnol.* **2011**, 583929.
37. Hingorani, S. R.; Wang, L.; Multani, A. S.; Combs, C.; Deramaudt, T. B.; Hruban, R. H.; Rustgi, A. K.; Chang, S.; Tuveson, D. A. Trp53R172H and KrasG12D cooperate to promote chromosomal instability and widely metastatic pancreatic ductal adenocarcinoma in mice. *Cancer Cell* **2005**, *7*, 469-483.
38. Weiss, W. A.; Aldape, K.; Mohapatra, G.; Feuerstein, B. G.; Bishop, J. M. Targeted expression of MYCN causes neuroblastoma in transgenic mice. *EMBO J.* **1997**, *16*, 2985-2995.
39. Jamin, Y.; Tucker, E. R.; Poon, E.; Popov, S.; Vaughan, L.; Boulton, J. K.; Webber, H.; Hallsworth, A.; Baker, L. C.; Jones, C.; Koh, D. M.; Pearson, A. D.; Chesler, L.; Robinson, S. P. Evaluation of clinically translatable MR imaging biomarkers of therapeutic response

- in the TH-MYCN transgenic mouse model of neuroblastoma. *Radiology* **2013**, *266*, 130-140.
40. Hosea, N. A.; Collard, W. T.; Cole, S.; Maurer, T. S.; Fang, R. X.; Jones, H.; Kakar, S. M.; Nakai, Y.; Smith, B. J.; Webster, R.; Beaumont, K. Prediction of human pharmacokinetics from preclinical information: comparative accuracy of quantitative prediction approaches. *J Clin. Pharmacol.* **2009**, *49*, 513-533.
41. CardiacProfiler, Eurofins Pharma Discovery Services. <http://www.eurofins.com/pharma-services/pharma-discovery-services/services/in-vitro-pharmacology/ion-channels.aspx>.
42. Hu, H.; Kolesnikov, A.; Riggs, J. R.; Wesson, K. E.; Stephens, R.; Leahy, E. M.; Shrader, W. D.; Sprengeler, P. A.; Green, M. J.; Sanford, E.; Nguyen, M.; Gjerstad, E.; Cabuslay, R.; Young, W. B. Potent 4-amino-5-azaindole factor VIIa inhibitors. *Bioorg. Med. Chem. Lett.* **2006**, *16*, 4567-4570.
43. Mineno, T.; Kansui, H.; Yoshimitsu, H. A convergent synthesis of the imidazopyridine scaffold of fluorescent alkaloid ageladine A. *Tetrahedron Lett.* **2011**, *52*, 3131-3132.
44. Kabsch W. Xds. *Acta Cryst. D* **2010**, *66*, 125–132.
45. Evans, P. R. Scaling and assessment of data quality, *Acta Cryst. D* **2006**, *62*, 72–82.
46. Emsley P.; Cowtan K. COOT: Model-building tools for molecular graphics. *Acta Cryst. D* **2004**, *60*, 2126–2132.
47. Bricogne G.; Blanc E.; Brandl M.; Flensburg C.; Keller P.; Paciorek W.; Roversi P.; Sharff A.; Smart O. S.; Vonrhein C.; Womack T. O. BUSTER, version 2.10.1; Global Phasing Ltd.: Cambridge, United Kingdom, 2012.

48. Adams, P. D.; Afonine, P. V.; Bunkóczi, G.; Chen, V. B.; Davis, I. W.; Echols, N.; Headd, J. J.; Hung, L.-W.; Kapral, G. J.; Grosse-Kunstleve, R. W.; McCoy, A. J.; Moriarty, N. W.; Oeffner, R.; Read, R. J.; Richardson, D. C.; Richardson, J. S.; Terwilliger, T. C.; Zwart, P. H. PHENIX: a comprehensive Python-based system for macromolecular structure solution. *Acta Cryst D* **2010**, *66*, 213–221.
49. Smart O. S.; Womack T. O.; Sharff A.; Flensburg C.; Keller P.; Paciorek W.; Vonrhein C.; Bricogne G. GRADE, version 1.2.1; Global Phasing Ltd.: Cambridge, United Kingdom, 2012.
50. Bruno, I. J.; Cole, J. C.; Kessler, M.; Luo, J.; Motherwell, W. D. S.; Purkis, L. H.; Smith, B. R.; Taylor, R.; Cooper, R. I.; Harris S. E.; Orpen, A. G. Retrieval of crystallographically-derived molecular geometry information, *J. Chem. Inf. Comput. Sci.* **2004**, *44*, 2133–2144.
51. Workman, P.; Aboagye, E. O.; Balkwill, F.; Balmain, A.; Bruder, G.; Chaplin, D. J.; Double, J. A.; Everitt, J.; Farningham, D. A.; Glennie, M. J.; Kelland, L. R.; Robinson, V.; Stratford, I. J.; Tozer, G. M.; Watson, S.; Wedge, S. R.; Eccles, S. A.; Committee of the National Cancer Research Institute. Guidelines for the welfare and use of animals in cancer research. *Br. J. Cancer* **2010** *102*, 1555-1577.

## TABLE OF CONTENTS GRAPHIC

